2016

Rheology and filtration of mono- and bi-disperse settling suspensions

Tejaswi Soori
Iowa State University

Rheology and filtration of mono- and bi-disperse settling suspensions

by

Tejaswi Soori

A thesis submitted to the graduate faculty

in partial fulfillment of the requirements for the degree of

MASTER OF SCIENCE

Major: Engineering Mechanics

Program of Study Committee:
Thomas Ward III, Major Professor
Wei Hong
Jonathan D. Regele

Iowa State University

Ames, Iowa

2016

DEDICATION

I dedicate this work to my mother Dr. Indira Jathi and my father Mr. Pradeep Soori for their love and support.

TABLE OF CONTENTS

Page

LIST OF FIGURES

NOMENCLATURE

$H(t)$ = Height of the fluid top interface (m)

H_0 = Height corresponding to capillary pressure loss (m)

$H_{bot}(t)$ = Height of the top of cake layer (m)

H_{cmax} = Maximum height of the cake layer after sedimentation (m)

C_{P_f} = Dynamic permeability correction for filter medium

$C_{P_{c+f}}$ = Dynamic permeability correction for cake layer & filter

C_{P_c} = Dynamic permeability correction for cake layer

C_1 = Superficial velocity due to stokes flow(m/s)

C_0 = Coefficient for Stokes flow though a 3D square channel geometry

k_f = Permeability of filter medium (m^2)

k_c = Permeability of cake layer (m^2)

$\bar{k}$ = Effective permeability (m^2)

ρ_f = Fluid phase density (kg/m^3)

ρ_S = Solid phase density (kg/m^3)

ρ_{pd} = Packing density

ϵ = Void fraction (porosity)

μ_f = Fluid phase dynamic viscosity(kg/ms)

μ_{cf} = Viscosity of calibration fluid (cSt)

μ_{susp} = Relative viscosity of suspension (kg/ms)

ω = Rate of cake layer formation

b = Width of settling tube (m)

A = Cross sectional area of settling tube (m^2)

$H(0)$ = Initial Height of fluid top interface (m)

ΔP_{cap} = Capillary pressure loss (N/m^2)

Q = Fluid flow rate (m^3/s)

ϕ = Total solid concentration (%)

ϕ_M = Maximum packing density (%)

d_p = Solid glass particle diameter (m)

α = Ratio of Width of settling tube v/s particle diameter

β = Fraction of small particles concentration in bi-disperse suspension (%)

ΔP_{hs} = Hydrostatic pressure difference (N/m^2)

ΔP_f = Pressure loss due to filter medium (N/m^2)

ΔP_c = Pressure loss due to cake layer (N/m^2)

ΔP_{total} = Total pressure loss experienced during gravity filtration (N/m^2)

τ = Shear stress on the fluid (N/m^2)

r_1 = Radius of outer cylinder (m)

r_2 = Radius of inner cylinder (m)

v_x = Velocity of moving plate in positive x-direction (m/s)

Ω = Uniform angluar velocity of rotating outer cylinder $(1/s)$

ACKNOWLEDGEMENTS

I would like to thank my major professor and research advisor Dr. Thomas Ward for his patient guidance, encouragement and valuable suggestions during the course of this research, without which this study would not have been possible. I would like to thank Mengyu "Allen" Wang for his assistance in conducting this research work and Andrew R. White for all his valuable suggestions during the course of this research . I would like to thank Dr. Wei Hong, for being a part of my Program of Study committee and for shared his knowledge in solid mechanics during my course work which helped me in understanding topics like rheology and viscous behaviors. I will take this opportunity to thank Dr. Jonathan D. Regele, who also agreed to be in my Program of study committee. I also want to thank the Department of Aerospace Engineering at Iowa State University for providing me the financial support in the form of Graduate Assistant position.

ABSTRACT

Rheological properties are of great interest in oil & gas, pharmaceutical, food, plastics and cosmetic industries which process different types of multi-phase suspensions. Review of existing literature on rheological studies and experiments are conducted to verify the effect of total solid concentration ϕ on the viscosity of mono-disperse and bi-disperse suspensions.

Gravity filtration involves flow of fluid through a porous filter medium and a time dependent cake layer which act as additional filter media. Filtration rate and cake build up as a function of time are examined for mono- and bi-disperse suspensions through theory and experimentation. Darcy's Law, which describes fluid flow through porous media, was applied along with the Kynch theory of sedimentation, which provides the basis for analyzing low concentration ($\phi \leq 0.1$) cake formation. Experiments were performed to study the effects of varying particle sizes ($45\ \mu\text{m} \leq d \leq 1400\ \mu\text{m}$) and total solid concentration ϕ on both the formation rate of the cake layer and its flow permeability (k) in conjunction with the filter media. Two CCD cameras were used to capture images of the cake formation and fluid drainage processes, and subsequent image and theoretical analysis found a constant pressure loss due to the permeability of the filter media, whereas the pressure loss due to the cake formation varies as a function of time, ϕ and d.

THESIS ORGANIZATION

In chapter 1, Section 1.1 will be a introduction to rheology of mono- and bi-disperse settling suspensions. Section 1.2 will provide a brief literature review of previous milestones and acclaimed research done on rheological studies of suspensions. In Section 1.3, we will discuss the experimental procedure, analysis, results, discussion and conclusion. Chapter 2 is a manuscript titled 'Gravity filtration of settling suspensions: Darcy-Washburn sedimentation model' in preparation for submission to the Journal of Powder Technology and will contain its own introduction, theory, experimental procedure, results, discussion and conclusion. Future prospects in this field will be presented in chapter 3 followed by a bibliography for the entire thesis.

CHAPTER 1. RHEOLOGY OF SUSPENSIONS

1.1 Introduction

A suspension is a multi-phase system with solid particles dispersed in liquid or gas phase and different varieties of suspensions are used in oil & gas, bio-chemical, food and pharmaceutical industries. In rheology, measuring effective viscosity of a suspension has always been a challenging topic. The difficulty in understanding the flow behavior of suspension arises due to the fact that, unlike simple fluids like water or air(Newtonian fluids), suspensions are governed by a wide range of parameters like relative particle size, total solid concentration, geometrical parameters of the particles, etc.

Viscosity arises due to collision between neighboring particles in a fluid which move at different velocities. When we consider a flow of fluid in a tube, the fluid near the wall moves slower than near the tube axis. At the walls, there is a no slip condition that exists which means fluid velocity at the walls is zero. This is shown in Fig. 1.1(a) Fig. 1.1(b)shows the velocity and shear stress profile when the top plate is moving in positive x direction with a velocity v_x, where h is the distance between the top and bottom plate. Here, the bottom plate is stationary. The shear stress $\tau = \mu dv_x/dy$ where μ is the dynamic viscosity of the fluid under study.

1.2 Literature Review

The study of rheology of suspensions was initially started by Einstein [1, 2] who proposed a basic formula to calculate the relative viscosity of suspensions which contain low

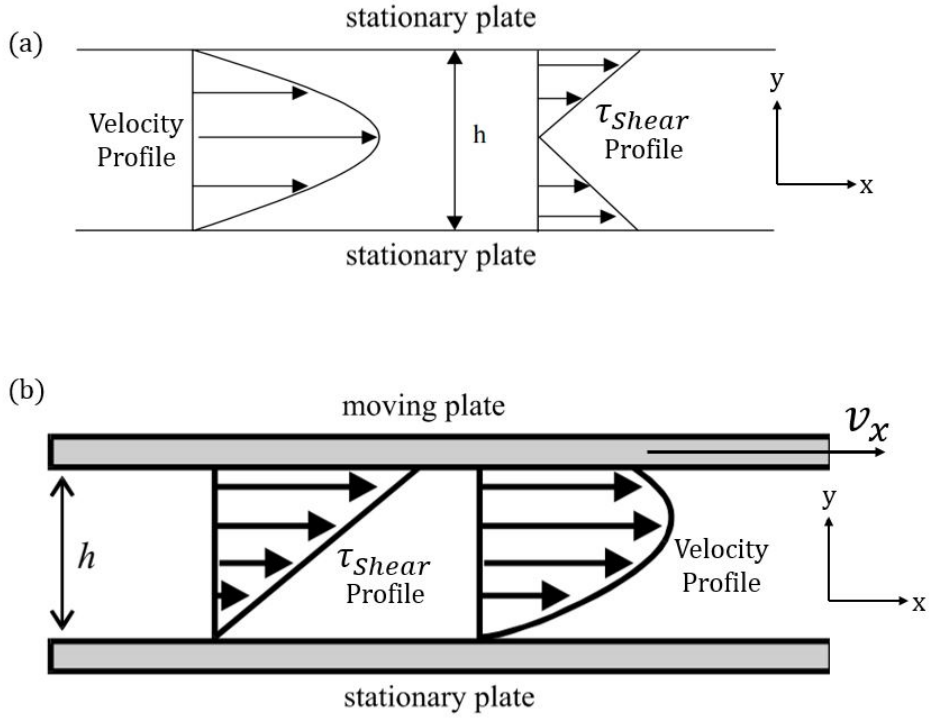

Figure 1.1: (a) Schematic of fluid flow between two parallel stationary plates which can be generalized to fluid flow in a tube. (b)Schematic showing the principle of couette viscometry with top plate moving in positive x-direction at velocity v_x and the bottom plate is stationary.

solid concentrations of uniform spherical particles. Later Chong, Christiansen and Baer [3], Eilers [4], Vand [5] developed theories and tried to extend Einstein's equation to suspensions with higher solid concentrations. But, the resulting equations, both theoretically and empirically, are different from each other. This is true for experimental data of high concentration suspensions too. This difference may be attributed to large range of particle size distributions of the mono-disperse particles, which results in change in total solid concentration for each study.

There are a lot of experimental and theoretical papers published on high-shear-limit viscosity of suspensions of uniform spherical particles and almost all of them show that the relative viscosity tends to infinity asymptotically as the solids volume fraction approaches

a maximum packing fraction, ϕ_M and this strong increase in viscosity is ascribed to the decrease in inter-particle distance. However, agreement between different data sets on the value of the maximum packing fraction is poor. A value of 0.53 is indicated but the data of Lewis and Nielsen [6] and Shapiro and Probstein [7], while de Kruif *et al.* [8] reports it to be equal to 0.71. Hence Shapiro and Probstein suggested that there exists a range of maximum packing fractions, with a lower bound of about 0.53. A well known model that explains the packing fraction of bi-disperse mixture was proposed by Ouchiyama and Tanaka [9] which estimates the packing density of a sphere packing by using statistical theory. The equation given in their work can be modified to calculate ϕ_M of the solid phase and has been used by Gupta *et al.* [10] and Poslinski *et al.* [11]. Fig. 1.2 shows the predicted value of packing density for bi-disperse mixture as stated by Shapiro and Probstein model.

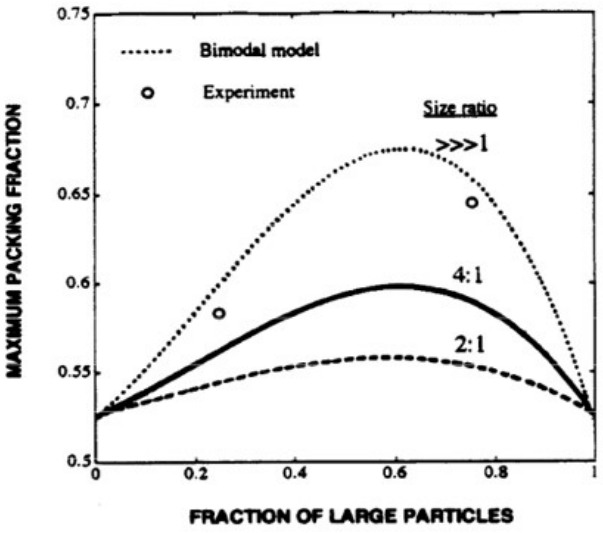

Figure 1.2: Packing density of bi-disperse mixture as predicted by Shapiro and Probstein in 1992.

Extending these equations to bi-disperse suspensions which contain two different particle species whose relative particle size is known, has been tried by numerous scholars but has been unsuccessful till date. It is easy to geometrically increase the limiting concentrations

which arise in mono-disperse suspensions by using the multi-disperse suspensions where there is a opportunity to pack smaller particles in the interstices of bigger particles. This is possible when we know the experimental values of blend ratios which is relative concentration of one species to other and size ratios, when we consider a bi-disperse suspension where there are two particle species of different size, there seems to be discontinuities in extending the mono-disperse suspension equations to bi-disperse suspensions.

Fidleris and Whitmore [12] studied the settling velocity of a large sphere in a mono-disperse suspension of low concentration $\phi = 0.2$ containing small particles, where the size ratio of small particles to the large particle in focus was 1/10 or less. From their experiments they observed that the large sphere encountered the same resistance to motion when passing through the suspension as when it passed through a pure liquid of the same viscosity and density as the suspension. Chong, Christiansen and Baer [3], Struik, Bree and Schwarzl [13] and Wildemuth and Williams [14] also observed this phenomena in their studies.

Farris [15] and Mooney [16]predicted the behavior of viscosity of bi-disperse suspension using the data available from studies done by previous scholars on mono-disperse suspensions. He developed a set of equations which considered the range of relative particle size and concentration to generalize the mono-disperse viscosity data to predict the viscosity of bi-disperse suspensions. In his literature, we can observe a particular total concentration ϕ and fraction of small particles within the bi-disperse mixture β where the relative viscosity of the bi-disperse suspension attains a minimum and this minimum has been attributed to efficient packing density and this has been proved in literatures by Qi and Tanner [17], Spangenberg *et al.* [18], Gondret and Petit [19] and many more scholars [20, 21, 22, 23].

Konijn *et al.* [24] conducted experimental study on parameters like solid fraction ϕ, particle diameter d and liquid viscosity μ_f which is similar to the study we have conducted, and

found that commonly used relations for the viscosity of suspensions are oversimplified and due to this, it is difficult to make direct comparison of experiments with different particulate and/or liquid materials in a quantitative manner. In this study, we try to experimentally validate that there indeed is a minimum relative viscosity for bi-disperse suspensions of a known total solid concentration ϕ. White and Walton [25] predicted that spherical particles of equal size may be packed in five different ways and calculated their theoretical void percentage. Fig. 1.3 shows their predicted orientations and their corresponding void fractions in %. This study was experimentally verified by McGeary [26].

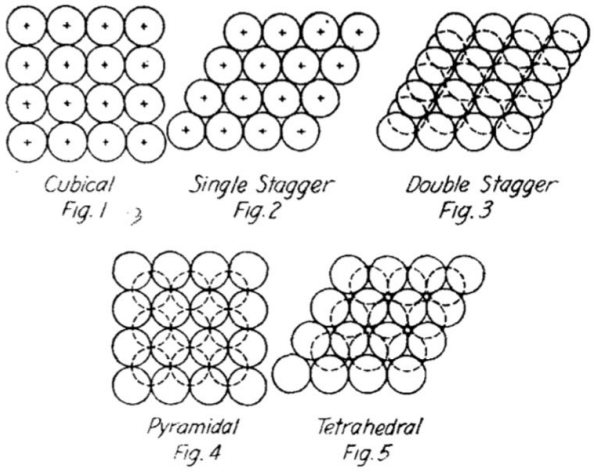

Fig. No.	Type of packing of spheres	Unit prism (Vol.)	Voids (%)
1	Cubical	$8r^3$	47.64
2	Single stagger (cubical tetrahedral)	$4r^3\sqrt{3}$	39.55
3	Double stagger	$6r^3$	30.20
4	Pyramidal	$4r^3\sqrt{2}$	25.95
5	Tetrahedral	$4r^3\sqrt{2}$	25.95

Figure 1.3: Orientations of equal size spherical particles and their corresponding void fractions predicted by Walton and White in 1937.

1.3 Experiments

Mono-disperse suspensions of known volume $V = 170$ mL containing glycerol manufactured by Fisher Scientific and spherical glass particles manufactured by Ceroglass Tech-

nologies Inc. of $d_1 = 850$ μm and $d_2 = 125$ μm respectively, and density $\rho_S = 2.54$ g/cm^3 were created by varying the total solid concentration ϕ. The suspensions were prepared by weighing the amount of glycerol and glass particles according to their relative concentration and density. Later these suspensions were stirred vigorously to avoid particles settling down to the bottom and to ensure uniform distribution of particles throughout the background fluid.

Similarly, bi-disperse suspensions of same volume V were created using glycerol and glass particles of two different diameter $d_2 = 125$ μm and $d_3 = 75$ μm for two concentrations $\phi = 0.4$ and 0.5. The bi-disperse suspensions for $\phi = 0.4$ were made such that the relative concentration of the two particle species used were varied with respect to each other. This was achieved by introducing a parameter β which is the measure of fraction of small particles in the total concentration bi-disperse mixture. So, for $\phi = 0.4$ and 0.5, β ranges from 0 to 1.

To measure the rheological properties of the pure glycerol fluid and prepared suspensions, we use Model 900 viscometer manufactured by OFITE Testing Equipment, Inc. This version of the viscometer is a true Couette coaxial cylinder rotational oilfield viscometer, which uses a transducer to measure the induced angle of rotation of the bob by a fluid sample. To make the process of measuring the rheological properties fully automated for control and data acquisition, the viscometer can be connected to a computer via a serial (RS-232) port using ORCADA software. To start measuring the viscosity of different materials, the viscometer should be calibrated using the calibration fluid supplied with the viscometer and the calibration fluid is Polydimethylsiloxane Silicone Oil of viscosity ($\mu_{cf} = 100$ cSt). We measure the temperature of the calibration fluid and insert the temperature v/s viscosity data into the fluid manager in the software. Next, we add approximately 170 mL calibration fluid into the clean and dry stainless steel sample cup and place it onto the platform. The lock nut is opened and the platform is raised until the fluid reaches the scribed line on the

rotor and then the lock nut is tightened. Temperature of the calibration fluid equalizes after a couple of minutes. Then we use the software and run the viscometer at different shear rates to calibrate the equipment.

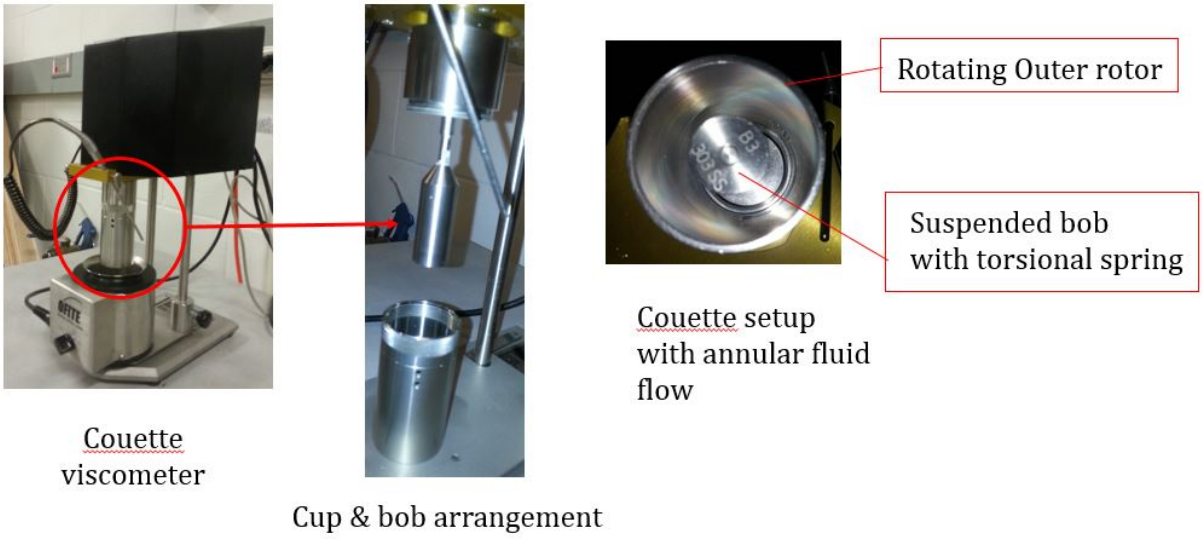

Figure 1.4: Couette viscometer used to measure the relative viscosity of bi-disperse suspension in the laboratory. The annular region between the outer and inner cylinder can be seen in the third image where the rotating outer cylinder is a rotor and inner cylinder is a suspended bob connected to a torsional spring.

Once the viscometer is calibrated, approximately 170 mL of mono- or bi-disperse suspensions was inserted into the sample cup of the OFITE viscometer. The lock nut is opened and the platform is raised again till the fluid reaches the scribed line on the rotor. We make sure that the suspension is well mixed before raising the platform to ensure uniform dispersion of particles and avoid any particles from settling. Then we set the shear rates on the software and gather data related to the suspension like shear stress, dynamic viscosity & temperature.

The principle of Couette viscometry is similar to fluid flow between a moving top plate and a stationary bottom plate or vice versa. In a Couette viscometer, the fluid flows between two coaxial cylinders of radii r_1 and r_2 where $r_1 > r_2$. The outer cylinder with radius r_1 is

rotated at a uniform angular velocity Ω and the torque experienced by the inner cylinder is converted to shear stress and then this shear stress is used to calculate the viscosity of the fluid. This conversion from torsion to viscosity is done by quantifying the torsion experienced by the torsional spring connected to the inner cylinder by using a transducer which senses the amount of torsion experienced by the spring. So, for a known amount of deformation in the spring, we have a calibrated data which can calculate the viscosity corresponding to the fluid under study. Fig. 1.4 shows the viscometer that we use to measure the relative viscosity of bi-disperse suspensions.

1.4 Results and discussion

Fig. 1.5 shows plot of suspension viscosity μ_{susp} v/s fraction of small particles in the mixture β for total solid concentrations of $\phi = 0.4$ and 0.5 for a bi-disperse suspension containing particle species of sizes d_2 and d_3. In this figure we can observe that for a given total solid concentration ϕ, there is a β value at which the relative viscosity of the suspension reaches a minimum, and the μ_{susp} v/s β curve tends to become more drastic as we increase ϕ. This observation is in agreement with the trend predicted by Farris[15].

1.5 Conclusion

From the study conducted above, we were able to obtain the numerical values of relative viscosity for bi-disperse suspensions of total solid concentrations $\phi = 0.4$ and 0.5 by varying the fraction of small particles present in the bi-disperse mixture β. We studied the bi-disperse suspensions of particle species whose sizes were $d_2 = 125$ μm and $d_3 = 75$ μm. We were able to experimentally validate that there indeed is a minimum relative viscosity for a bi-disperse suspension of hard spherical particles predicted by Farris [15] and this minimum viscosity is dependent on the size ratio of the two particle species in consideration. While

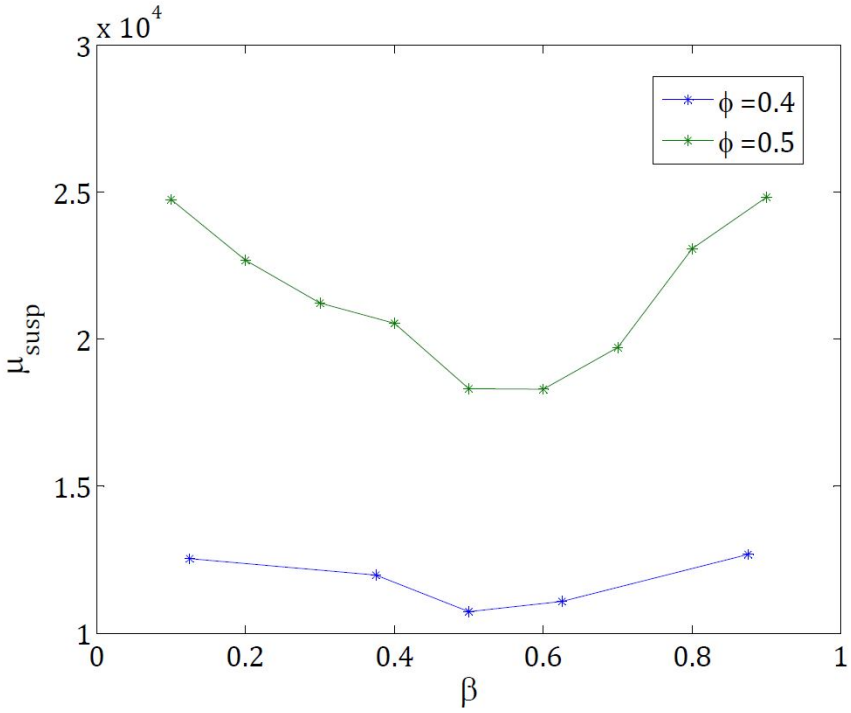

Figure 1.5: Plot of bi-disperse suspension relative viscosity μ_{susp} v/s fraction of small particles in the mixture β for total solid concentrations of $\phi = 0.4$ and 0.5 containing particle species of sizes $d_2 = 125$ μm and $d_3 = 75$ μm.

Einstein's studies are able to predict the viscosity of low concentration suspensions of spherical particles, the same study cannot be used to calculate the relative viscosities of dense suspensions and bi-disperse suspensions. We will need much more robust physical model to explain the behavior of rheology of dense suspensions and bi-disperse suspensions which will take into account numerous parameters like total concentration, particle size distribution, size ratio distribution of particle species, and many more which add to the difficulty of analyzing these systems.

CHAPTER 2. GRAVITY FILTRATION OF SETTLING SUSPENSIONS: DARCY-WASHBURN SEDIMENTATION MODEL

A paper in preparation for submission to the Journal of Powder Technology.

Tejaswi Soori, Mengyu Wang and Thomas Ward

2.1 Abstract

This paper examines the filtration rates of mono- and bi-disperse suspensions as a function of time and a cake layer builds up through theory and experimentation. Darcy's Law, which describes fluid flow through porous media, was applied along with the Kynch theory of sedimentation , which provides the basis for analyzing low concentration ($\phi \leq 0.1$) cake formation. Experiments were performed to study the effects of varying particle sizes (45 μm $\leq d \leq$ 1400 μm) and total solid concentration ϕ on both the formation rate of the cake layer and its flow permeability (k) in conjunction with the filter media. A CCD camera was used to capture images of the cake formation and fluid drainage processes, and subsequent image and theoretical analysis found the fluid flow experienced a constant pressure loss due to the permeability of the filter media, whereas the experienced pressure loss due to the cake formation varies as a function of time, ϕ and d. The rate of cake formation was also found to be independent of ϕ but dependent on d which can be attributed to a change in porosity affecting permeability.

2.2 Introduction

Settling suspensions when subjected to gravity filtration, we have a time dependent cake layer forming over the filter media due to sedimentation of solid particles and then there is fluid flow through those cake layers and the filter media and eventually the solid and liquid phase separation. The difficult part of this type of filtration is predicting the permeability of the cake layer whose thickness increases with time. What is interesting is that the height of this cake layer is a function of total solid concentration ϕ and for each concentration there is a specific height of the cake layer. Also, the permeability which is a measure of the ability of a porous material to allow fluid through it or a measure that quantifies the amount of open area in a porous material through which the filtrate can flow. Again this permeability is a function of total solid concentration and size of the particle species. So, for a bi-disperse suspensions where we have two different particle species of two different size, permeability will depend on their relative concentration and relative size. This makes the system very complex to analyze with simple techniques and tools.

Darcy [27, 28, 29] in his studies trying to understand physics behind porous media flow, developed a constitutive equation that describes the fluid flow through a porous media. His work was based on experimental results of water flow through sand beds which is a kind of porous media. Darcy's law states that the total fluid flux is equal to the product of permeability of the filter medium, the cross sectional area to flow and the pressure loss over the filter medium, all divided by the viscosity of the flowing fluid and the length of the filter medium.

$$Q = \frac{-kA(P_{x_2} - P_{x_1})}{\mu L}. \tag{2.1}$$

where Q is the fluid flux (m^3/s), k is the permeability of the porous media (m^2), A is the cross-sectional area to flow (m^2), $P_{x_2} - P_{x_1}$ is the pressure loss over the length of the filter medium, μ is the viscosity of the fluid and L is the length of the filter medium.

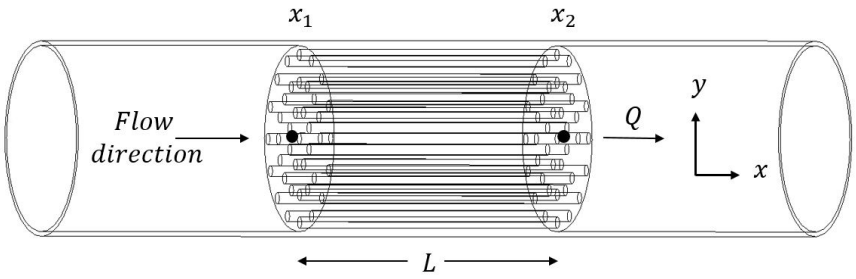

Figure 2.1: Simple schematic of darcy flow through a porous medium.

In 1921, Edward Washburn [30] developed a equation that describes capillary flow in a bundle of parallel cylindrical tubes. In this study, a porous media is generalized as a bundle of capillaries closely placed to each other. Both Darcy Law and Washburn equation are altitude dependent and need modification if elevation is considered because pressure is proportional to liquid height.

Most of the studies on sedimentation of suspended particles have been based on findings of Kynch [31]. He provided the methods to determine the sedimentation rates by assuming that a first order partial differential equation controlled the entire sedimentation process where he used: (1) continuity balance & (2) sedimentation velocity as a function of total solid concentration. A general solution in the form of total solid concentration $\phi_s = f(x - vt)$ was determined by Kynch and his theory was based on the propagation of sedimentation waves in a suspension and the sedimentation was regarded as a process of concentration changes traveling upwards from the bottom a settling tube due to movement of solids in the downward direction. Tiller [32] made a revision to Kynch theory of sedimentation claiming that Kynch ignored the sediment or cake rising from the bottom of the settling chamber,

and derived new equation based upon the assumption that the characteristics emanate from the rising sediment. Similar studies on batch sedimentation were also done by [33, 34, 35]

Gravity filtration of suspensions is used to obtain the cake resistance at low pressure under laboratory conditions. Important study to derive governing equation for gravity filtration of suspension has been done by Tiller, Hsyung and Cong [36]. However their experiments were done using kaolin clay as the solid phase in the suspension whose size is very small compared to our studies. Wakeman [37] studied the influence of particle properties on filtration by considering the effect of particle size distribution,shape, size & interaction with the surrounding fluid and found that these properties have a profound effect on constitutive property(specific resistance) of the cake layer that in turn affects filter performance. He concluded that if the particle property could be user specified for a filtration, one should have particles as large a size as possible, as near to spherical as possible and have a mono-size distribution. Sørensen, Moldrup, and Hansen [38] and Bürger, Concha and Karlsen [39] studied similar systems but replacing the gravity with pressure by exerting it using a impermeable barrier(piston). Important literature that explains filtration with sedimentation by applying Kynchs theorem was proposed by Font and Hernández [40] who concluded that it is possible to apply the fundamentals developed for the sedimentation batch test to filtration batch process if some modifications are included.

Tien, Bai and Ramarao [41] did a study on the effect of smaller particle on the cake growth and filtration process and determined that local permeability reduction of a filter cake results from two factors: cake consolidation & cake clogging and the even if the amount of small particles is small, its effect on permeability can be substantial. Kavoosi [42] in his thesis has determined the permeability for standard size filter mediums by experimental analysis. França, Massarani and Biscaia [43] used the dynamic experimental batch sedimentation data to estimate the parameters of cake permeability by studying the constitutive

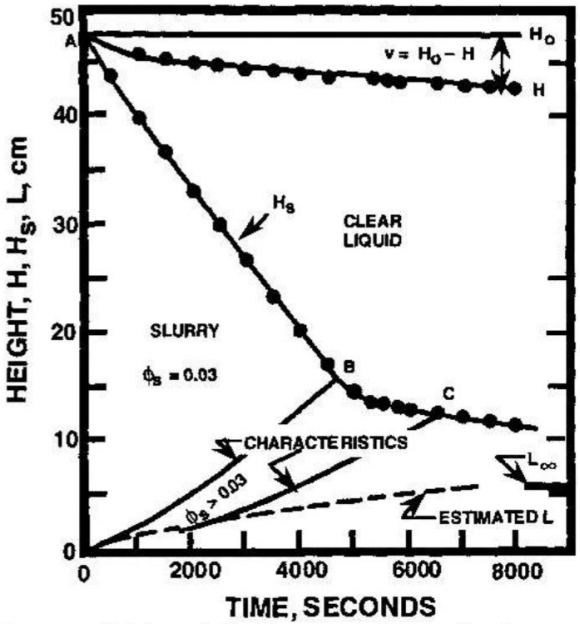

Figure 2.2: Study by Tiller, Hsyung and Cong on $\phi = 0.03$ by volume suspension of kaolin clay. In this plot, we can clearly see the top interface height, the Kynch line of characteristics and the concentration front traveling downwards.

equations which characterize a porous medium.

Lu *et al.* [44] found in their study that: (i) At a given position in a cake, the solid compressive pressure reaches a maximum value and then decreases for a gravity filtration due to the decrease in the driving head, (ii) A cake constructed with bi-disperse mixture has a more compact structure than does one with mono-disperse particles and (iii) A bi-disperse suspension with higher β value has lower cake porosity and higher specific cake resistance. Numerical model of gravity filtration of slurries was done by Christensen and Keiding [45] and they suggested that the filtration rates are highly dependent on the resistance offered to fluid flow by the deposited material, i.e., the cake. Also, the cake resistance is a function of cake height and average specific cake resistance. Bargieł and Tory [46] used particle-based approach to simulate the sedimentation of poly-disperse suspensions and predicted that the final solids concentration can vary from 0.55 to 0.64 for uniform spheres. Their study says that ϕ_M increases with decreasing increasing tube width to particle size ration α which is in

agreement with the results obtained in our experiments.

Studies similar to this paper was also done by Hernando, Omari and Reungoat [47] where they did experimental investigation of batch sedimentation of concentrated bi-disperse suspensions with $\phi = 0.3$ using a laser-induced fluorescence technique but their study focuses more on particles of different density and particle size ratio. Grenier *et al.* [48] analyzed the flux decline in dead-end filtration by using a phenomenological approach, which includes a qualitative identification of the main fouling mechanisms which affect the filter media. However, since the filter opening is smaller than the particle size in consideration of our study, this is of less importance to us. But however, if we were to look at smaller particles, this study would help in understanding how the filter medium is clogged.

Textbooks on solid-liquid separation by Rushton *et al.* [49], Svarovsky [50] discuss general filtration methods like cross flow, deep bed filtration etc. But, the importance of gravity filtration will arise when we need to determine the permeability of the cake layer at low pressure as suggested by Ripperger *et al.* [51]. Similar studies on filtration and sedimentation were also done by a lot of other scholars [52, 53, 54, 55, 56].

Using these previous studies, we have conducted the study to understand the gravity filtration process of mono- and bi-disperse suspensions and developed a governing equation that explains the filtration of low concentration suspensions while determining numerically the *dynamic* permeability correction for filter, cake and the height corresponding to the capillary pressure loss.

2.3 Theory

Consider an initially well mixed nearly mono-disperse particle laden fluid. The fluid phase properties are the density and viscosity denoted ρ_f and μ_f, respectively. The particle diameter and density are denoted d_p and ρ_S, respectively. The suspension is poured into a square tube with a filter at the bottom with permeability k_f. The filter pores are smaller than the particle diameter such that the liquid and solid content separate. Over time a cake layer builds up which has a time dependent permeability denoted k_c. After some time the liquid and solid content are separated.

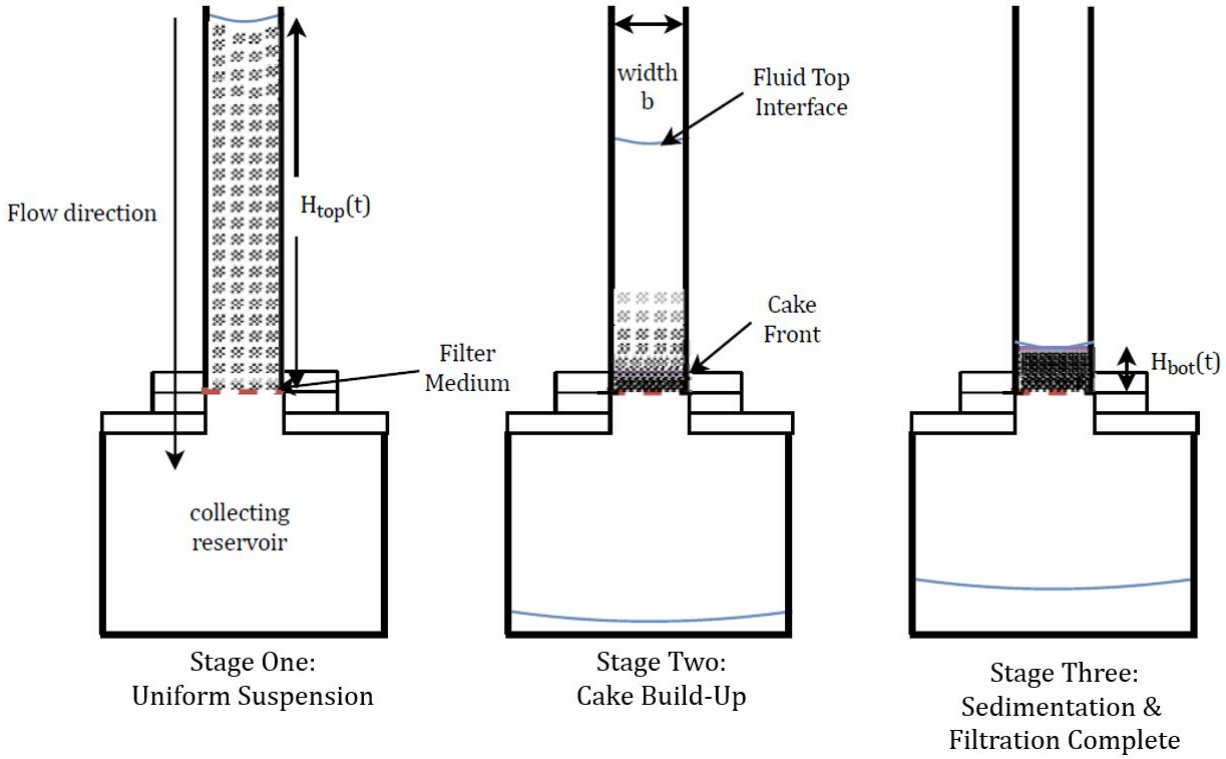

Figure 2.3: Stages of gravity filtration of suspensions: Stage 1 shows the settling tube containing suspension with uniformly dispersed particles and height H at time $t = 0$. Stage 2 shows the settling tube at time $t > 0$ where the fluid top interface has traveled downwards and the cake layer building up over the filter medium. Finally at stage 3 we can see that the sedimentation of particles dispersed initially have settled down completely and the filtration of the background fluid is complete.

In Fig. 2.3, H(t) is the height of the fluid top interface in the settling tube and is a function of time. 'b' is the width of the settling tube. H_{bot} is the height of the cake interface which is zero at $t = 0$. At t > 0, there are three zones within the settling tube, 1) Clear fluid zone where there is no presence of particles, 2) Transition zone where the concentration of particles in the top area is less than 'ϕ' and in the bottom area is greater than 'ϕ' within this zone, 3) Cake layer of height H_{bot} which builds up until all the particles dispersed in the liquid phase settle down and reaches a maximum height H_{cmax} . After complete sedimentation, the fluid filters out through the cake layer and the filter media.

2.3.1 *Darcy-Washburn sedimentation model*

According Darcy's law [27, 28, 29], the fluid flux through the square cross sectional area $A = b^2$ of the tube assuming a three-dimensional geometry is $Q/A = dH/dt = C_0[k/(H\mu)] \sum \Delta P$. Here $C_0 = 0.42$ is the coefficient when considering Stokes flow though a three dimensional channel of square geometry [57] and $\sum \Delta P = \Delta P_{hs} + \Delta P_f + \Delta P_{c+f}$ where ΔP_f & ΔP_{c+f} are both functions of time. In the model we are proposing there is a capillary pressure due to the filter $H_0 = \Delta P_{cap}/(\rho g)$ and pressure losses due to the filter and particles ΔP_f & ΔP_{c+f} respectively which reduces the flow rate.

Kynch theory of sedimentation [31] explains the sedimentation process for low concentration suspensions ($\phi \leq 0.1$). Based on this theory, height of the cake layer interface $H_{bot}(t)$ is defined as:

$$H_{bot}(t) = H_{cmax}(1 - e^{-\omega t}). \tag{2.2}$$

where H_{cmax} is the final height of the cake layer.

For gravity filtration, the hydrostatic pressure difference has the form:

$$\Delta P_{hs} = -\rho g(H - H_0). \tag{2.3}$$

where ΔP_{hs} is negative in nature since the hydrostatic pressure is measured at the bottom of the tube.

The resistance to fluid flow due to the filter medium is a function of time as mentioned above, and has the form:

$$\Delta P_f = \frac{-12Q\mu H_0}{C_0 k_f A} \tag{2.4}$$

and due to the cake layer is also a function of time, and has the form:

$$\Delta P_{c+f} = \frac{-12Q\mu H_0}{C_0 \bar{k} A} \tag{2.5}$$

where, $\bar{k}$ which is the effective permeability obtained by lumping the permeability of the filter and the permeability of the cake layer and is expressed as:

$$\frac{1}{\bar{k}} = \frac{1}{k_c} + \frac{1}{k_f}. \tag{2.6}$$

This means:

At t = 0, resistance to flow is due to ΔP_f and

As t $\rightarrow \infty$, resistance to flow is due to ΔP_{c+f}.

In other words, at time t = 0, the fluid experiences resistance to flow due to the filter medium only because of the absence of any cake layer. Whereas, for time t $\rightarrow \infty$, the fluid experiences resistance to flow due to both the filter medium and the cake layer.

Both ΔP_f & ΔP_{c+f} are actually positive (resistance) since Q is negative. The total pressure loss ΔP_{total} is positive because ΔP_f or ΔP_{c+f}, depending on time, dominate the hydrostatic pressure ΔP_{hs}. So,

$$\Delta P_{total} = \frac{12Q\mu(H - H_0)}{C_0 A^2}. \tag{2.7}$$

Now equating

$$\Delta P_{total} = C_{P_f}\Delta P_f e^{-\omega t} + C_{P_{c+f}}\Delta P_{c+f}(1 - e^{-\omega t}) + \Delta P_{hs}. \tag{2.8}$$

we get:

$$\frac{12Q\mu(H - H_0)}{C_0 A^2} = -\frac{12Q\mu H_0 C_{P_f} e^{-\omega t}}{C_0 k_f A} - \frac{12Q\mu H_0 C_{P_{c+f}}(1 - e^{-\omega t})}{C_0 \bar{k} A} - \rho g(H - H_0). \tag{2.9}$$

After rearranging the terms and simplifying we arrive at the following equation:

$$\frac{dH}{dt} = \frac{H_0}{H}\frac{dH}{dt}\left[1 - \left[C_{P_c} + \left(\frac{AC_{P_f}}{k_f} - C_{P_c}\right)e^{-\omega t}\right]\right] - C_1\frac{(H - H_0)}{H}. \tag{2.10}$$

where $C_1 = \rho g A C_0/12\mu$ and $C_{P_c} = AC_{P_{c+f}}/\bar{k}$.

The constants $C_{P_{c+f}}$ & C_{P_f} corresponds to *dynamic* permeability corrections for the cake layer and filter, respectively. The fluid viscosity and density are denoted by μ and ρ, respectively and are independent of the dispersed phase properties. The variable ω represents the rate of formation of the cake layer. Note that for $\omega = 0$, the flow rate is determined by the pressure loss due to the filter only and after integration we arrive at the the analytical solution which is of the form:

$$\Delta t = -\frac{C_{P_f}}{C_1} H_0 \ln\left|\frac{H - H_0}{H(0) - H_0}\right| - \frac{1}{C_3}\left[H - H(0)\right]. \tag{2.11}$$

where $H(0)$ is the initial height of the fluid top interface in the settling tube.

2.4 Experiments

2.4.1 *Setup and procedure*

An acrylic tube of height $H = 16\ cm$ with a square geometry and internal side length $b = 1.53\ cm$ was used as the main settling tube. A 200 mesh filter seals off the lower end of the tube with the aid of acrylic adaptor pieces on the outside. A collection tank was placed underneath to capture the oil filtered through the media and the cake layer. Three fluorescent tubes provided lighting with two in front of and on either side of the experimental setup, and another light directly behind the tube to intensely illuminate the region of interest and provide a uniform background. While tracking the oil interface necessitated a wide field of view encompassing the entire settling tube, tracking the cake build up required a high resolution, zoomed-in view of the few centimeters immediately above the filter media. To accommodate these two conflicting sets of demands, two CCD cameras were used to capture images of the experiment. However, the images captured during filtration of bi-disperse suspension is not analyzed because different size particles settle at different speeds. So, tracking the top of the cake layer is hard to distinguish. To ensure that the proximity of the light sources does not have any thermal effect on the fluid in the system, we used a thermocouple and found both temperature variations in the room and additional heating introduced by the fluorescent tubes to be negligible for the first few experiments. Suspensions were poured into the settling tube, and images were captured till the completion of the filtration process. Fig. 2.4 shows the schematic of the experimental setup for gravity filtration of suspensions as seen from right side.

The background fluid used for the experiments was a high viscosity ($\mu_1 = 1000$ cSt) Polydimethylsiloxane Silicone Oil manufactured by Clearco Products Company with a den-

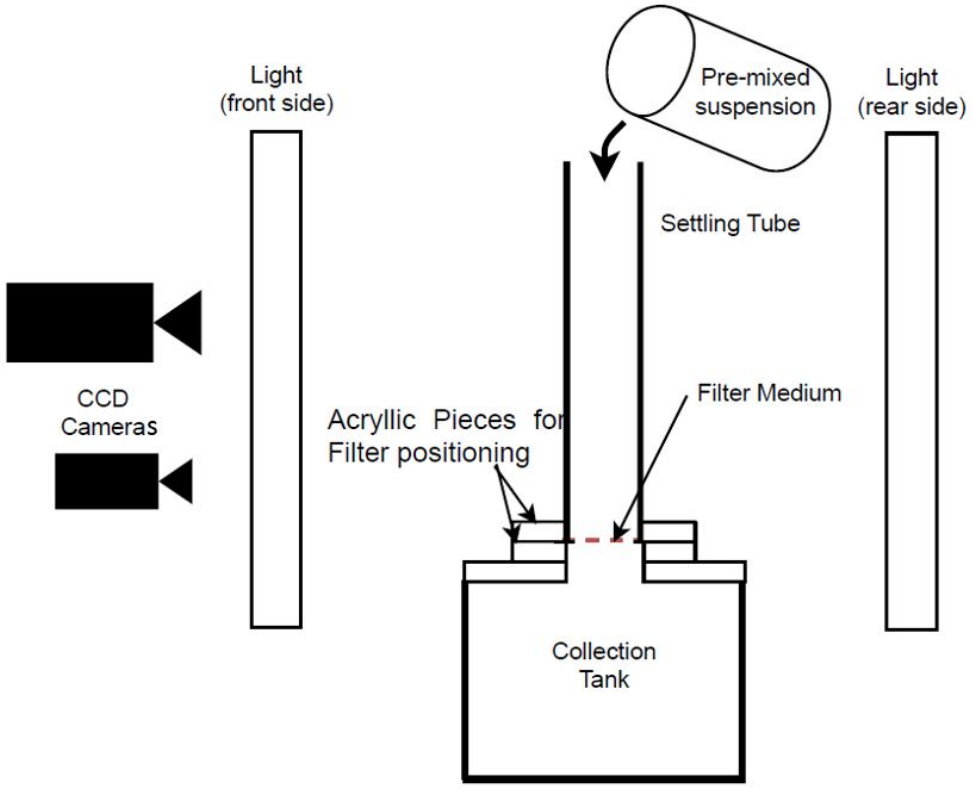

Figure 2.4: Schematic of the experimental setup. This figure shows a schematic view of the experimental setup. The two CCD cameras are placed in front of the settling tube to capture the fluid top interface and cake interface. The lights on the front side are placed such that the settling tube is illuminated and the rear side light is placed exactly behind the settling tube to help visualize the cake layer build up and to provide a sharp contrast to the fluid top interface. The filter medium is placed between two acrylic adaptor pieces which are then glued together to fix the filter position.

sity $\rho_f = 0.97$ g/cm^3. GSB grade 1, 6, and 9 glass particles manufactured by Ceroglass Technologies Inc. with a density of $\rho = 2.54$ g/cm^3 were selected. Individual particle sizes vary significantly across GSB grades (e.g. GSB 1 particles range from 12-20 mesh corresponding to 841 to 1680 μm). To increase size precision, particles were further sorted through sieves manufactured to ASTM (American Society for Testing and Materials) E-11 Specifications by Dual Manufacturing. Particles filtered through sieve numbers 12, 35, 60, but captured by sieve numbers 14, 40, 70 corresponding to diameters of $d_1 = 1410$-1680 μm, $d_2 = 420$-500 μm, $d_3 = 210$-250 μm were then selected. The particles were coated with ink and acetone

solution and dried in a oven to sharpen the contrast for imaging during sedimentation across concentration gradients and different size particles had different ink to distinguish the sedimentation in case of bi-disperse suspensions.

2.4.2 *Permeability Measurement*

Analytical and empirical studies have found that the void fraction of randomly packed particles in a cylindrical tube converge to ~ 0.4 with decreasing particle diameter. The volumes of three tubes were determined by measuring the mass of the tubes with and without water. Two tubes with a similar rectangular geometry, but different cross sectional areas of $A_1 = 23.409 \times 10^{-6}$ m^2 & $A_2 = 5.625 \times 10^{-6}$ m^2. A third rectangular with a similar cross-sectional area as A_2, but with sharper corners was also used for this set of experiments.

The void fractions were then evaluated across six particle sizes $d = 75$, 250 425, 1590, 3140 and 6250 μm for each tube. The densities of d_1, d_2, and d_3 were known, but the densities of d_4, d_5, and d_6 were measured experimentally. An electronic caliper was used to verify the particles diameters, from which their volumes were calculated. Sets of 20 particles would then be massed to minimize error in the scale and geometry of the particles. With their mass and volume known, their densities were determined.

The tubes were filled to overcapacity with beads, leveled off at the top, and then massed. The difference relative to the tubes empty mass divided by particle densities represent the volume occupied by the beads. With both the total volume and the occupied volume known, the void fractions were found to converge to ~ 0.45, slightly higher than that of cylindrical tubes [26].

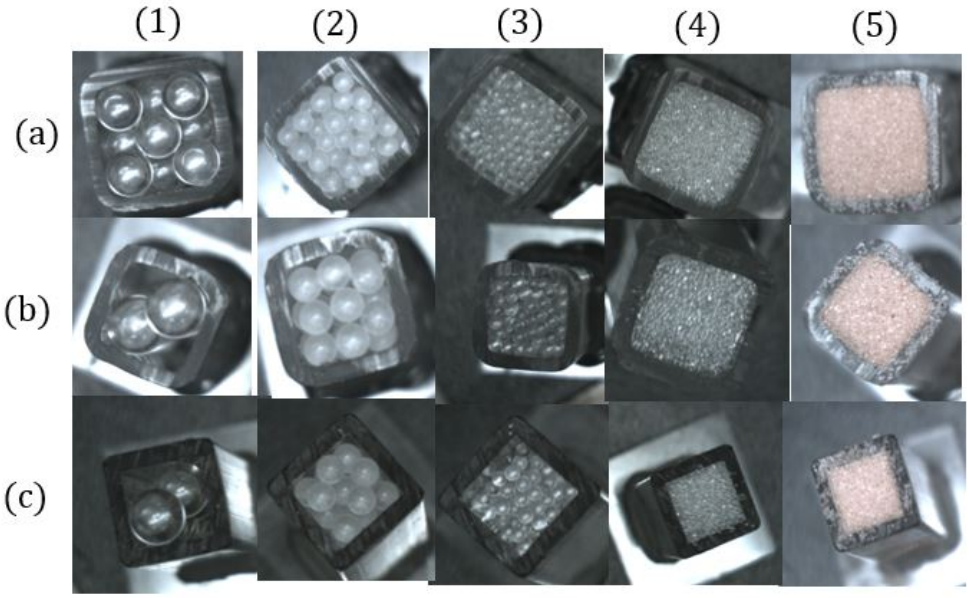

Figure 2.5: Row (a) shows the settling tube of cross sectional area A_1 with columns (1)-(5) depicting reduction of particle size, row (b) shows the settling tube of cross sectional area A_2 with columns (1)-(5) depicting reduction of particle size and row (c) shows the settling tube of cross sectional area A_2 with sharp corners with columns (1)-(5) depicting reduction of particle size. Column (1)-(5) correspond to particle size 5 mm, 2.5 mm, 1400 μm, 425 μm and 212 μm respectively.

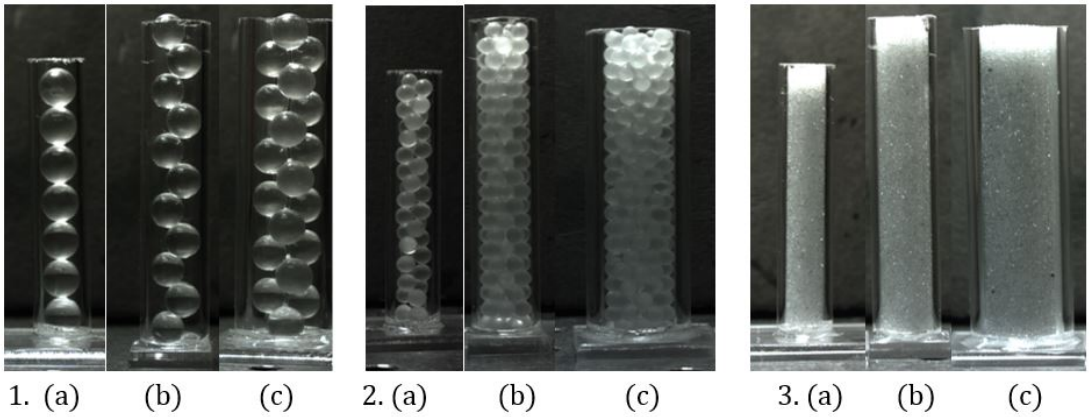

Figure 2.6: 1-3.(a) correspond to a circular cross sectional settling tube of internal diameter 6 mm, 1-3.(b) correspond to a settling tube of cross sectional area A_2 and 1-(c) correspond to a settling tube of cross sectional area A_1. In all these sets of figures, 1., 2. and 3. correspond to particle sizes 5 mm, 2.5 mm and 425 μm respectively. In these sets of figures we can actually see the voids which account to the void fraction(porosity).

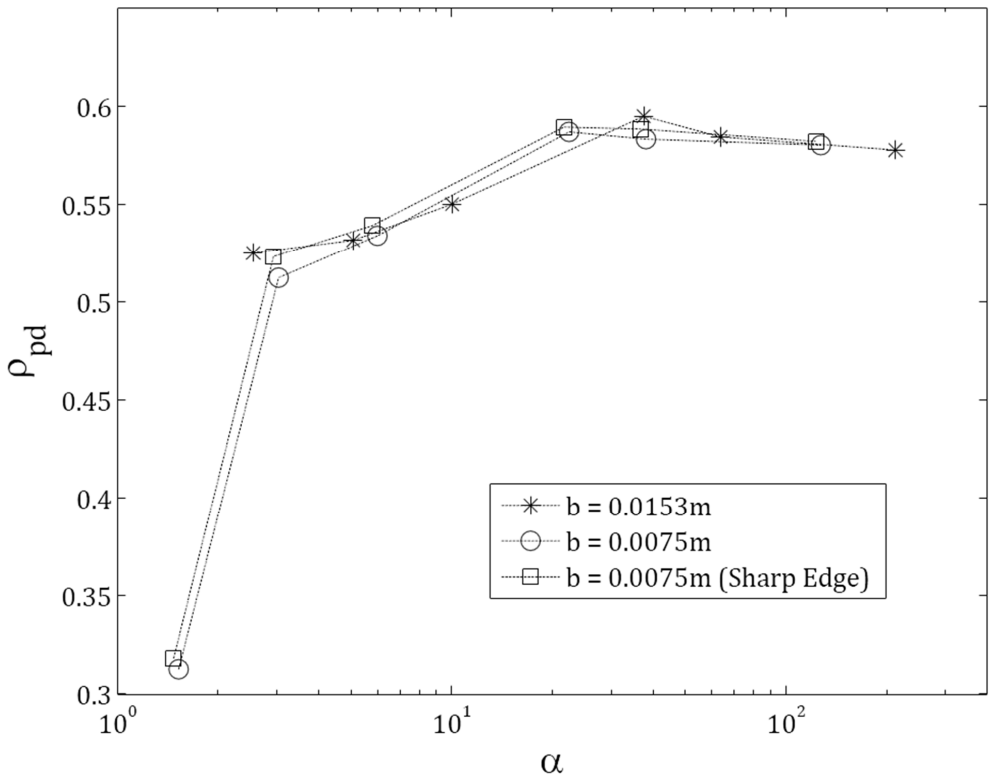

Figure 2.7: Semi-log plot of Packing ratio ρ_{pd} for glass beads of varying size expressed in terms of α which is a ratio of tube width and particle size in settling tubes of $A_1 = 23.409 \times 10^{-6} m^2$ & $A_2 = 5.625 \times 10^{-6} m^2$. The tube with sharp edge has a cross sectional area similar to A_2. From the figure it is to be noted that ρ_{pd} for α values corresponding to particle sizes 'd_1', 'd_2' & 'd_3' used in our experiments does not change significantly. This also means the value of void fraction(porosity) ϵ remains almost constant. Note: $\epsilon = 1 - \rho_{pd}$.

Fig. 2.7 shows a semi-log plot of Packing ratio ρ_{pd} for glass beads of varying size expressed in terms of α which is a ratio of tube width and particle size in settling tubes of $A_1 = 23.409 \times 10^{-6}$ m^2 and $A_2 = 5.625 \times 10^{-6}$ m^2. The tube with sharp edge has a cross sectional area similar to A_2. Scholars like Mueller [58] have studied the packing density in detail for randomly packed fixed beds of uniformly sized spheres in cylindrical containers.

2.4.3 *Gravity Filtration Setup and procedure*

Dynamic permeability correction C_{P_f} for filter medium is determined analytically by comparing the experimental value and numerical value where the latter is computed using Runge-Kutta method. A known volume of pure silicone oil of high viscosity ($\mu_1 = 1000$ cSt) is measured and subjected to filtration in the settling tube. Due to the absence of particles, the fluid experiences pressure difference due to filter alone, which is equivalent to flow fluid through porous media. The experimental H v/s t is generated and Eq. 2.11 is used to generate the numerical H v/s t curve. To confirm that the value obtained analytically is correct, the same process is repeated for pure silicone oil of viscosity ($\mu_2 = 100$ cSt).

Three sets of mono-disperse suspensions at a constant $\phi = 0.05$ and varying $d = d_1$, d_2, d_3 were prepared to study the effects of particle size variation. This process was repeated by keeping $\phi = 0.06$, 0.07, 0.08, 0.09 & 0.10 constant each time to study the effects of varying concentrations which resulted in a total 18 different mono-disperse suspensions. Particles would clump together when introduced to the background fluid, entrapping air bubbles. These clumps were broken up by vigorous stirring, and the concentration would be allowed to sit to allow time for the air bubbles released from clump break-up to dissipate. Immediately before beginning the experiment, the concentrations were then remixed by a gentle mechanical homogenization to minimize air bubble reintroduction.

Keeping $\phi = 0.07$ constant, we prepared three bi-disperse suspensions containing d_1 & d_2 where the fraction of d_2 in the total concentration was 0.25, 0.50 and 0.75 respectively and another three suspensions containing d_1 & d_3 where the fraction of d_3 in the total concentration was 0.25, 0.50 and 0.75 respectively. The above 6 bi-disperse suspensions were prepared to study the effect of particle size ratio and relative concentration of each particle species. Further three bi-disperse suspensions were prepared at $\phi = 0.08$ containing d_1 & d_2 where the fraction of d_2 in the total concentration was 0.25, 0.50 and 0.75 respectively to make sure

that there was agreement between mono-disperse and bi-disperse experiments with respect to increase in ϕ. Similar to mono-disperse suspensions, process of mixing the bi-disperse suspension to uniformly distribute the particles is followed.

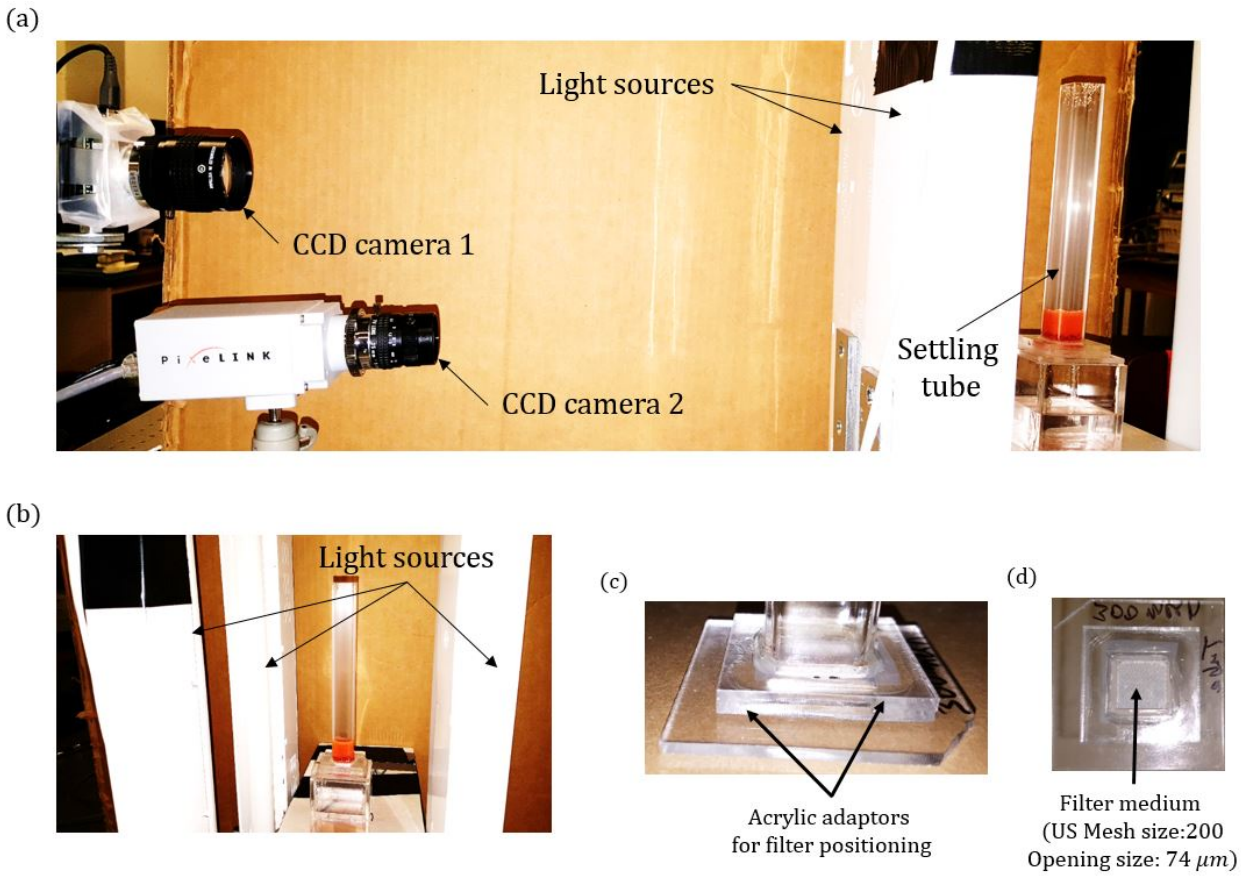

Figure 2.8: Experimental setup: (a) shows the actual laboratory experimental setup. Here, we can see the positions of the two CCD cameras of 'PIXELINK' make and (b) shows the side view of the tube and the light sources mentioned in Fig. 2.4.

2.5 Results and discussion

2.5.1 *Image analysis*

Fig. 2.9 shows different stages observed during gravity filtration of suspensions in the experimental setup. Stage 1 shows a empty settling tube. Stage 2 shows the settling tube containing a mono-disperse suspension of known ϕ at time $t = 0$ where particles are uniformly dispersed in the fluid phase. Stage 3 shows the settling tube at time $t > 0$ where we have the fluid top interface traveling downwards and a cake layer building over the filter media with all the variables marked. Stage 4 shows the settling tube when all the particles have settled down and Stage 5 shows the settling tube after complete filtration of the fluid. The images captured by CCD camera 1 is analysed using MATLAB to generate fluid top interface height v/s time. The fluid top interface is visible due to the sharp contrast created by the light source set up directly behind the settling tube which looks similar to stage 3 in Fig. 2.9. This interface is captured from the time $t = 0$ till the top interface reaches the bottom of the tube, which implies the filtration is complete. Since we know the width of the settling tube b, and the number of pixels it corresponds to in the image, we mathematically convert the number of pixels between top interface and bottom of the tube to a physical height of fluid top interface H in meters. Next, by using the time between each image, we can generate the $H\ v/s\ t$ data and use this method for all our experiments. Similarly we generate the height of the cake interface v/s time using the images captured by CCD camera 2. Now that we know $H_{bot}(t)$ and H_{cmax}, using Eq. 2.2 we compute the experimental value of ω, for all species of particles and concentration. It is to be noted that the experimental data deviates from numerical data obtained from Eq. 2.2 for $\phi\ > 0.1$. Fig. 2.13 shows a comparison between experimental data for H_{bot} v/s t obtained from image analysis and numerical data for H_{bot} v/s t obtained from solving Eq. 2.2 by specifying the value of ω and H_{cmax}.

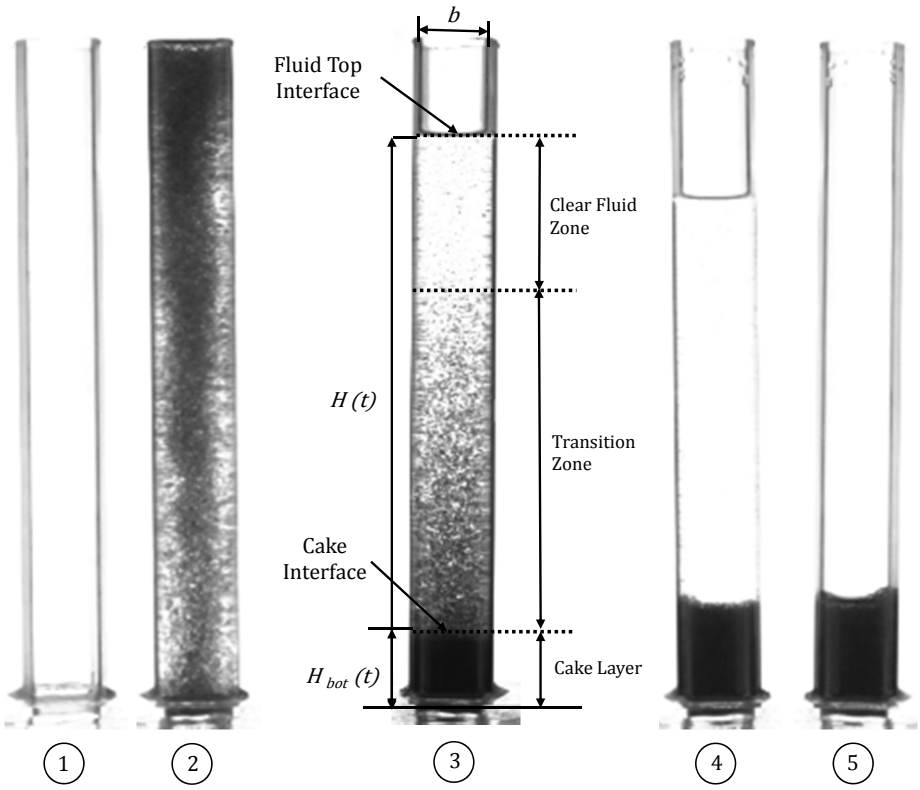

Figure 2.9: Observation of stages during experiments: Stage 1 shows the empty settling tube. Stage 2 shows the settling tube filled with mono-disperse suspension where particles are uniformly distributed at $t = 0$. In stage 3, we can see the fluid top interface traveling downwards and a thin layer of cake building up from the bottom. Stage 4 shows the settling tube after completion of sedimentation of particles. At this point, the cake layer has reached the maximum height H_{cmax}. Stage 5 shows the state of settling tube after completion of filtration.

To locate the fluid top interface and cake layer interface, images were subjected to threshold analysis where a search region is specified in the vicinity of the interface which is visible in the image due to sharp contrast. Then the minimum pixel value within that search region is found and the pixel number that corresponds to the minimum is the interface that we are tracking. This process is repeated to all the images in a loop while updating the search region continuously. Fig. 2.14 shows the threshold analysis of an image where we track the

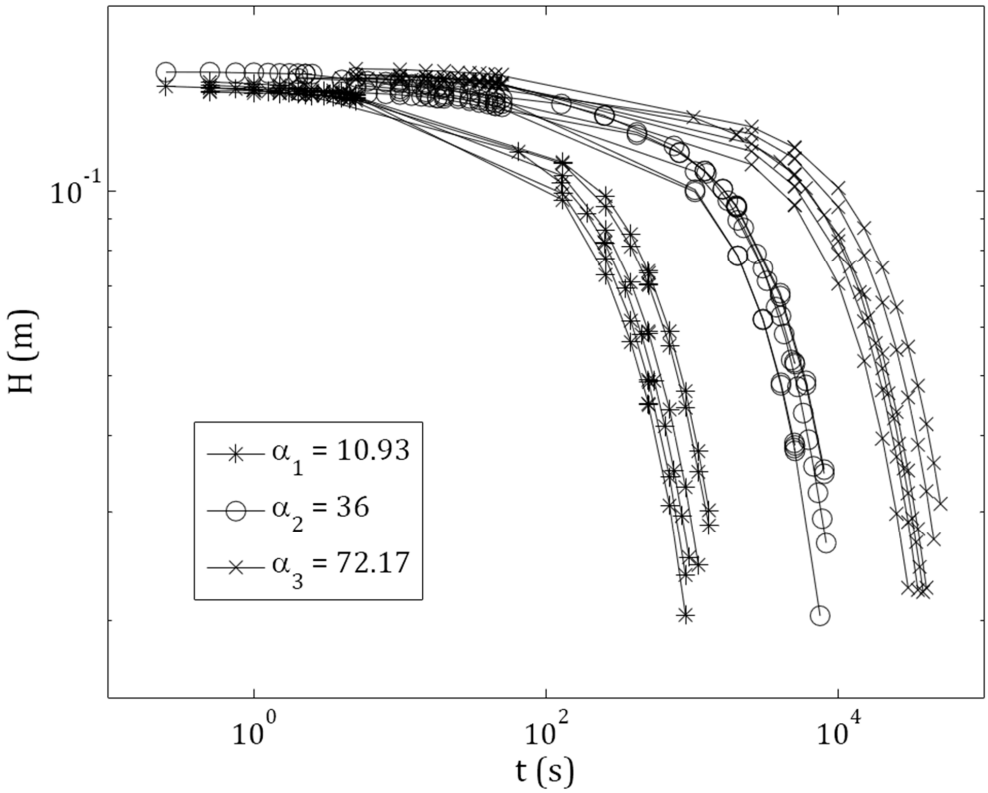

Figure 2.10: A log-log plot of Height of fluid top interface H v/s time t for mono-disperse suspensions of $10.93 \leq \alpha \leq 72.17$, at $0.05 \leq \phi \leq 0.10$.

top interface and Fig. 2.15 shows the similar process for an image where we track the bottom interface where we can see the shart change in average red value due to the sharp contrast created by the top interface and bottom interface.

The time between images was set with the intuition that suspensions of small particles would take longer to filter out, which means the rate at which the top interface would travel downwards is slower for smaller particles. Hence the capture time between two images was larger for smaller particles. However for bi-disperse suspensions, each species of particles had a unique rate of cake formation, hence it was impossible to collect the cake interface v/s time data and the experimental value of ω. Fig. 2.10 shows a log-log scale plot of H v/s t

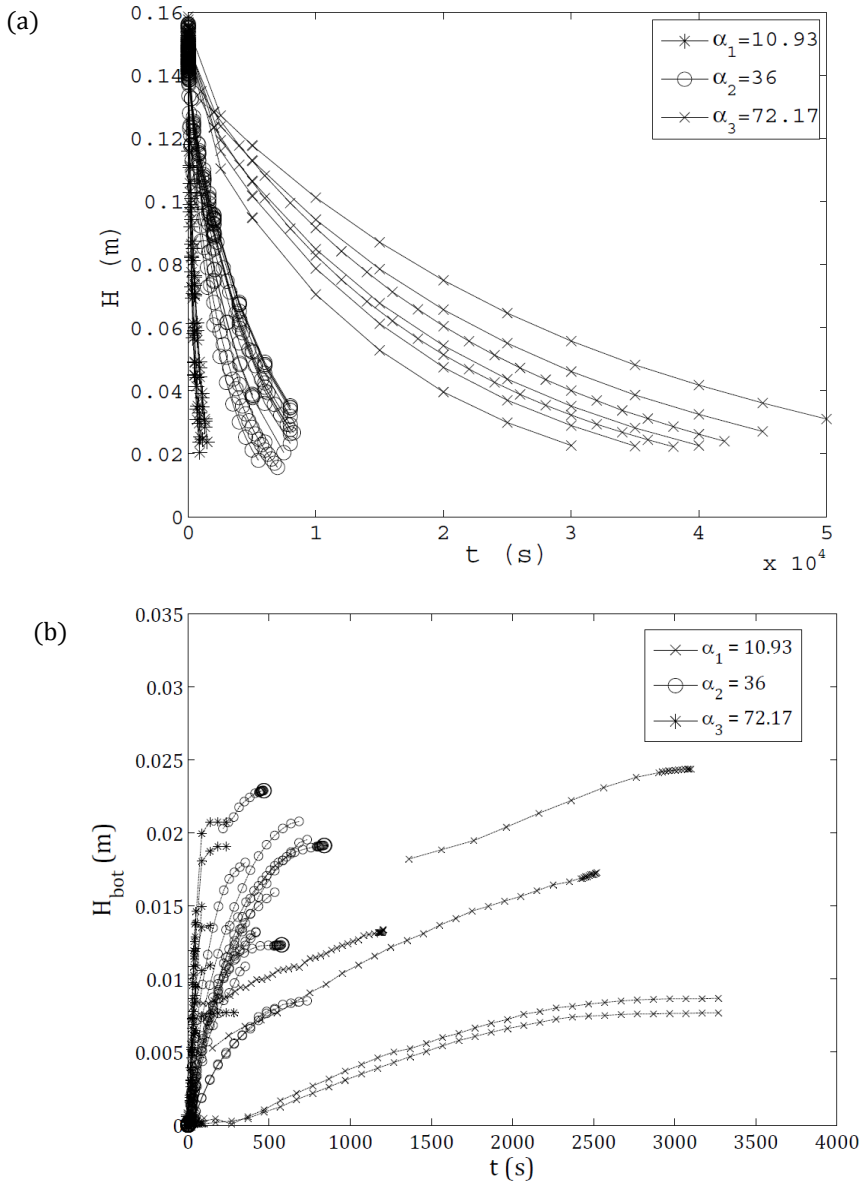

Figure 2.11: (a) shows the height H v/s t for different concentration and α values. (b) shows the height of cake layer H_{bot} v/s time t for mono-disperse suspensions of $10.93 \leq \alpha \leq 72.17$, at $0.05 \leq \phi \leq 0.10$.

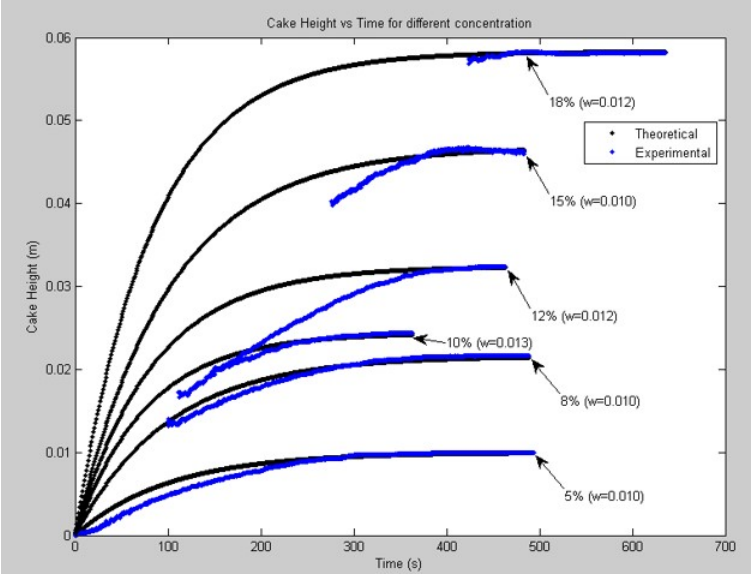

Figure 2.12: Deviation of experimental cake height H_{bot} v/s time t from the theoretical curve generated using Eq. 2.2 observed for concentrations $\phi > 0.1$.

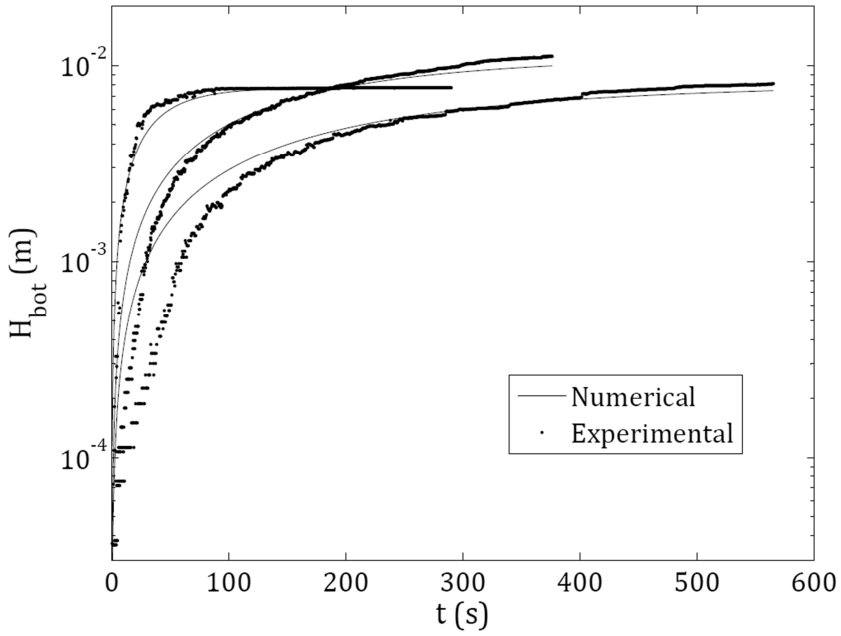

Figure 2.13: Semi-log plot of cake height H_{bot} v/s time t. A comparison of Experimental data and Numerical data obtained from Eq. 2.2.

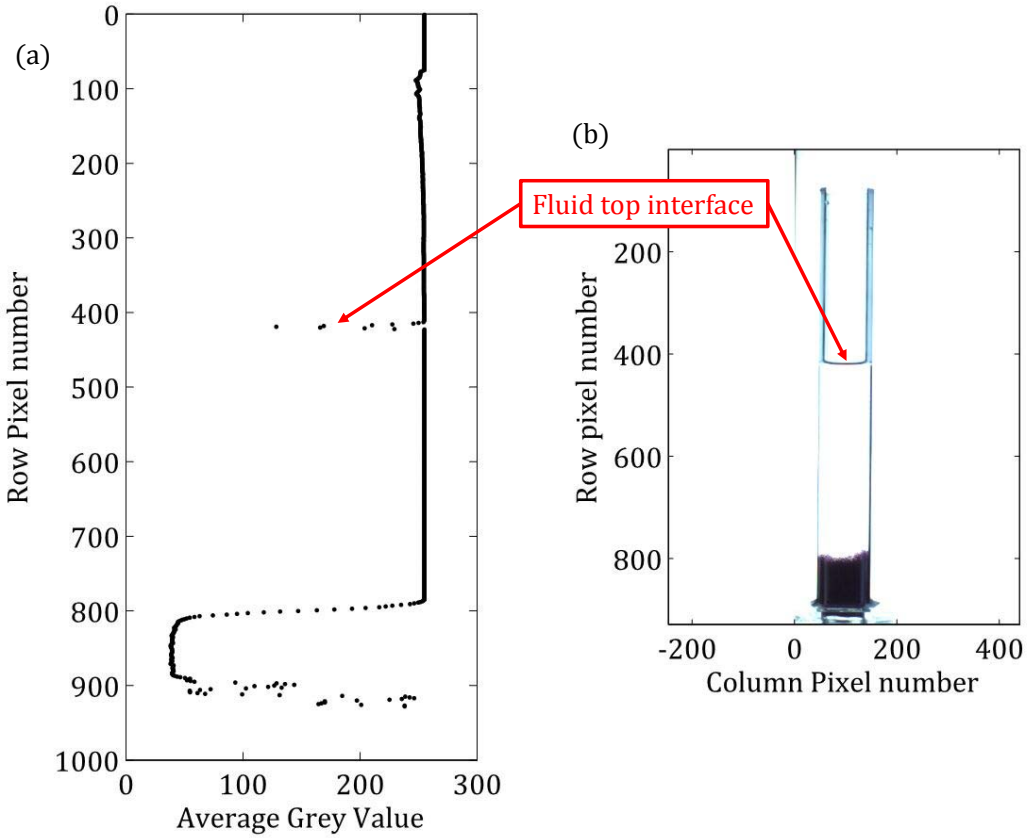

Figure 2.14: Threshold image analysis for top interface tracking using MATLAB. Fig. (a) shows the plot of averaged pixel value v/s the row pixel numbers of the image shown in Fig. (b).

obtained using the analysis method mentioned above from the images captured by CCD camera 1. Fig. 2.11 (a) shows typical H v/s t plot for $\phi = 0.05$ & 0.1 for α_1, α_2 and α_3 respectively where we can see the behavior of filtration height v/s time. Fig. 2.11 (b) is a plot of H_{bot} v/s t for mono-disperse suspensions of various α values. All the data from the image analysis is stored in a MATLAB data file which will be utilized to determine the value of *dynamic* permeability correction C_{P_c} and height corresponding to capillary pressure loss H_0 using pattern search algorithm which is explained below.

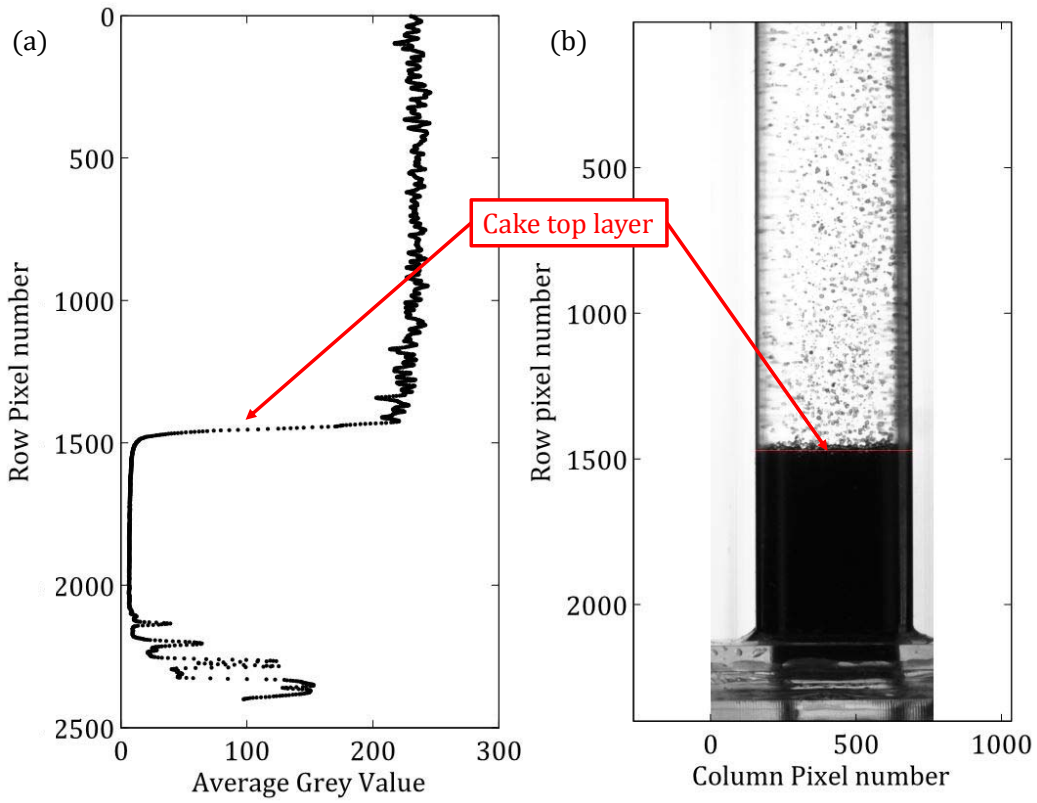

Figure 2.15: Threshold image analysis for cake layer interface tracking using MATLAB. Fig. (a) shows the plot of averaged pixel value v/s the row pixel numbers of the image shown in Fig. (b).

We used 2.11 to determine the numerical value of *dynamic* permeability correction for filter C_{P_f}. Pure silicone oils of $\mu = 1000\,cSt$ & $100\ cSt$ were individually subjected to filtration through US 200 mesh whose opening size was $74\,\mu m$, twice for each oil. Then the experimental height of fluid top interface H v/s time t was gathered.

This was done by generating experimental height of fluid top interface H v/s time t by subjecting pure silicone oils of dynamic viscosities $\mu = 1000\,cSt$ & $100\,cSt$ respectively to filtration through US 200 mesh of opening size $74\mu m$. Then we generated Numerical H

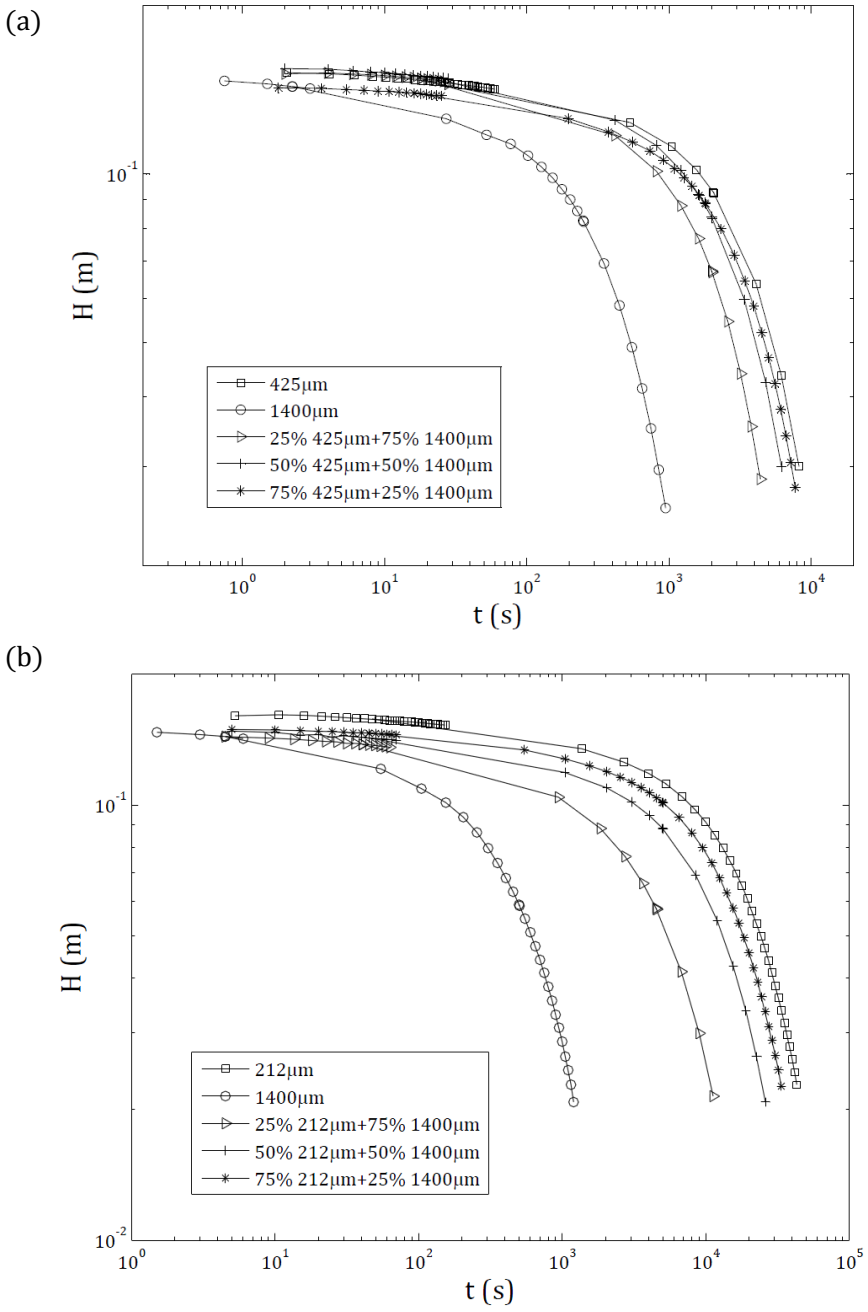

Figure 2.16: Log-log plots of Height of fluid top interface H v/s time t for bi-disperse suspensions with varying concentration ϕ and varying mixture of particle sizes.

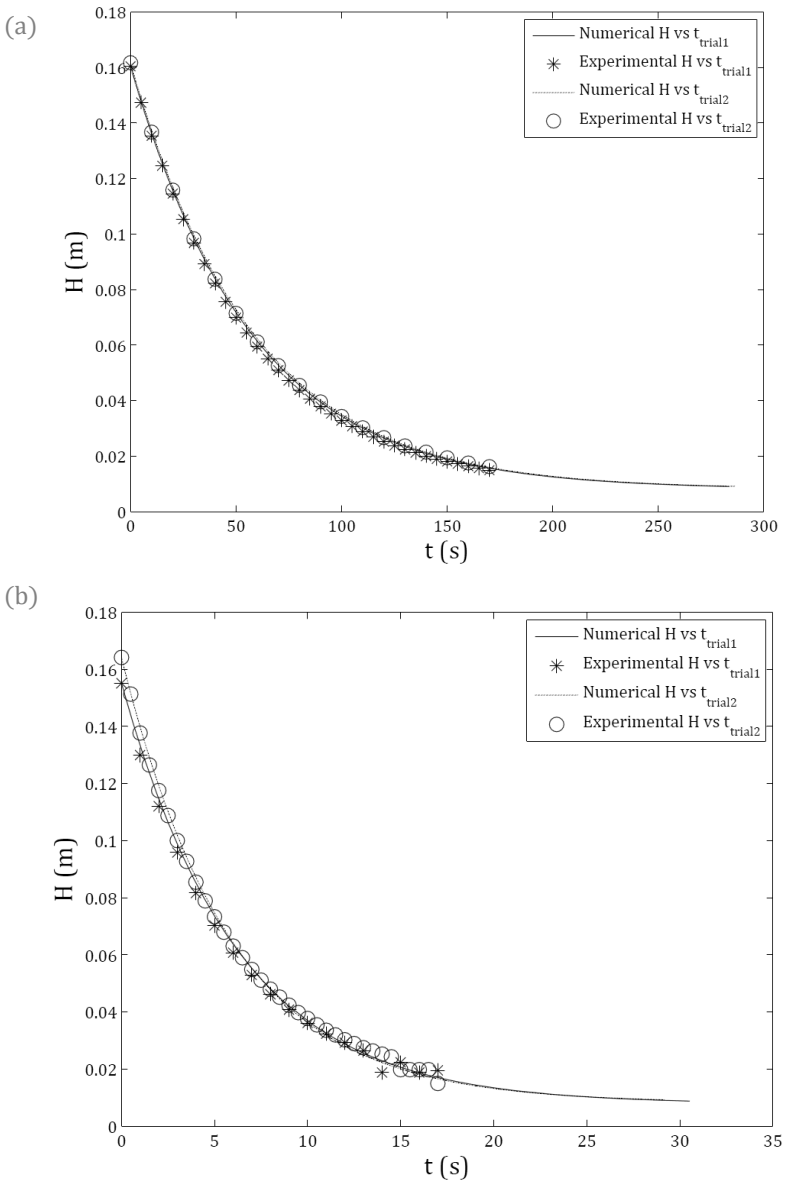

Figure 2.17: a) A comparison between experimental fluid top interface height 'H' v/s time 't' for pure silicone oil of $\mu = 1000$ cSt and numerical 'H' v/s time 't' behavior generated by using the analytical solution. b) Similar comparison with pure silicone oil of $\mu = 100$ cSt. Runge-Kutta 4^{th} order method is used to numerically determine the value of *dynamic* permeability correction for filter C_{P_f} which is equal to 0.1377. Here, '$\circ'$ & '$*'$ correspond to two different experimental runs and '—' &'$\cdots'$ correspond to numerical data for the two runs.

v/s t using Fig.2.17 (a) shows A comparison between experimental fluid top interface height 'H' v/s time 't' for pure silicone oil of $\mu = 1000\, cSt$ and numerical 'H' v/s time 't' behavior generated by using the Eq.2.11 analytical solution. Fig.2.17 (b) Similar comparison with pure silicone oil of $\mu = 100\, cSt$. Runge-Kutta 4^{th} order method is used to numerically determine the value of *dynamic* permeability correction for filter C_{P_f} which is equal to 0.1377. Here, '$\circ'$ & '$*'$ correspond to two different experimental runs and '—' &'$\cdots'$ correspond to numerical data for the two runs.

2.5.2 *Curve fitting: Pattern search algorithm*

Once we have the $H\ v/s\ t$ data after analysing all the experimental images, we use pattern search algorithm [59] which is a method of unconstrained numerical optimization used for efficient minimization of multiple unknown parameter. This method does not require the gradient of the problem to be optimized. Hence pattern search algorithm can be used on functions that are not continuous or differentiable. Such optimization methods are also known as direct-search, derivative-free or black-box methods. In our studies, there is no real way to estimate the actual value of *dynamic* permeability correction C_{P_c} and height corresponding to capillary pressure loss H_0 experimentally. So, we determine these two values numerically by curve fitting the objective function Eq. 2.10 to the experimental $H\ v/s\ t$ curve obtained from image analysis. The variables that we try to optimize are *dynamic* permeability correction C_{P_c} and height corresponding to capillary pressure loss H_0 and we start with a initial guess for both these variables to begin the pattern search. After each iteration of optimization, the objective function is evaluated to calculate the error to evaluate if the optimized values of the variables are the local minimums and if they are, the search region shrinks by a predefined factor and the pattern search goes through next iteration. This process is repeated until a global minimum is found for these two variables. Fig. 2.18 shows the trajectories followed by the pattern search method while optimizing the two variables C_{P_c} and H_0 for different

experimental data. Here we can observe the contours of error in the region ±25 % of the global minimum and the trajectories followed by the minimization for different initial guesses marked by black '∗' and all trajectories end at the same global minimum marked by black '×'.

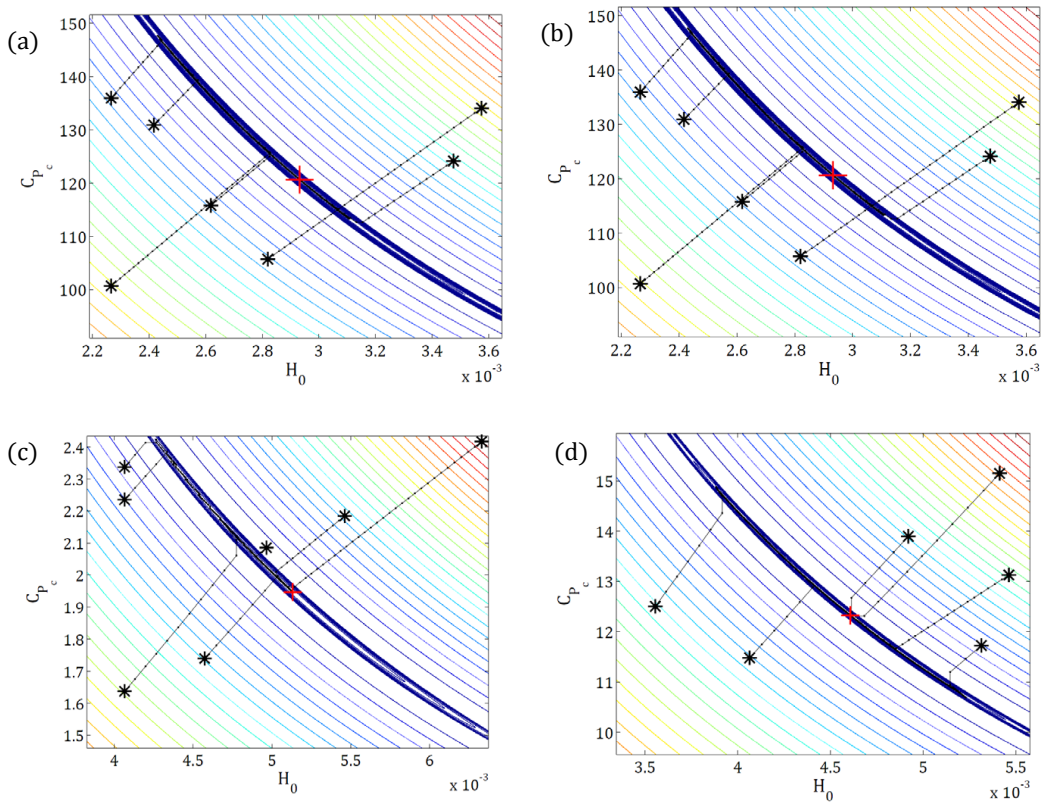

Figure 2.18: Plot of error contours generated during minimization of the objective function. The black lines with dark black dots show the projectiles of the pattern search method starting from a initial guess till it is optimized.

Fig. 2.19 (a) shows a semi-log scale plot of C_{P_c} v/s ϕ and Fig. 2.19 (b) is a plot of H_0 v/s ϕ for different mono-disperse particle species denoted by α_1, α_2 and α_3. Similarly Fig. 2.20 (a) shows a semi-log scale plot of C_{P_c} v/s ϕ and Fig. 2.20 (b) is a plot of H_0 v/s ϕ for bi-disperse suspensions of different particle combinations and these values are obtained from pattern search for all sets of experiments.

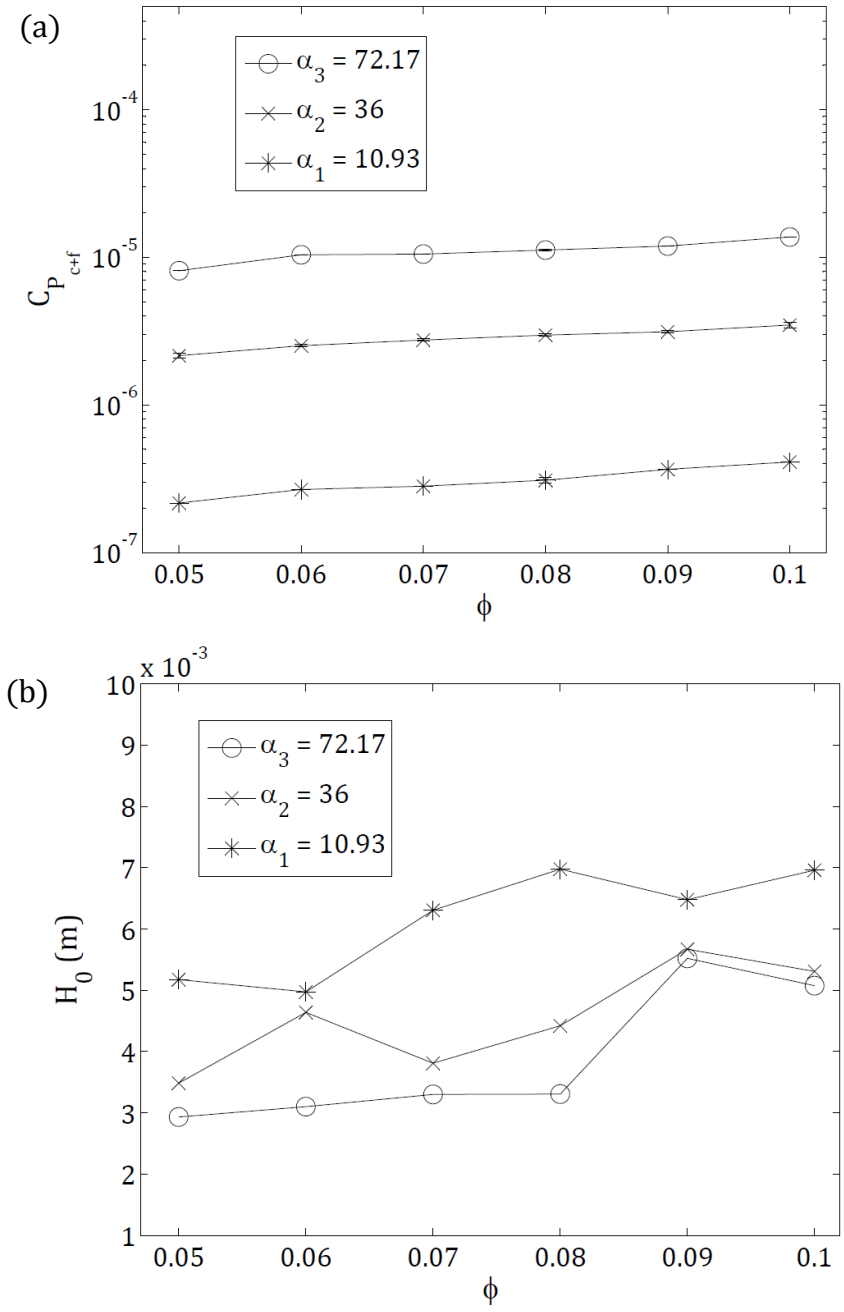

Figure 2.19: (a) Semi-log plot of *dynamic* permeability correction for cake $C_{P_{c+f}}$ for different 'α' v/s concentration ϕ. (b) Plot of Height corresponding to capillary pressure loss H_0 for different 'α' v/s concentration ϕ.

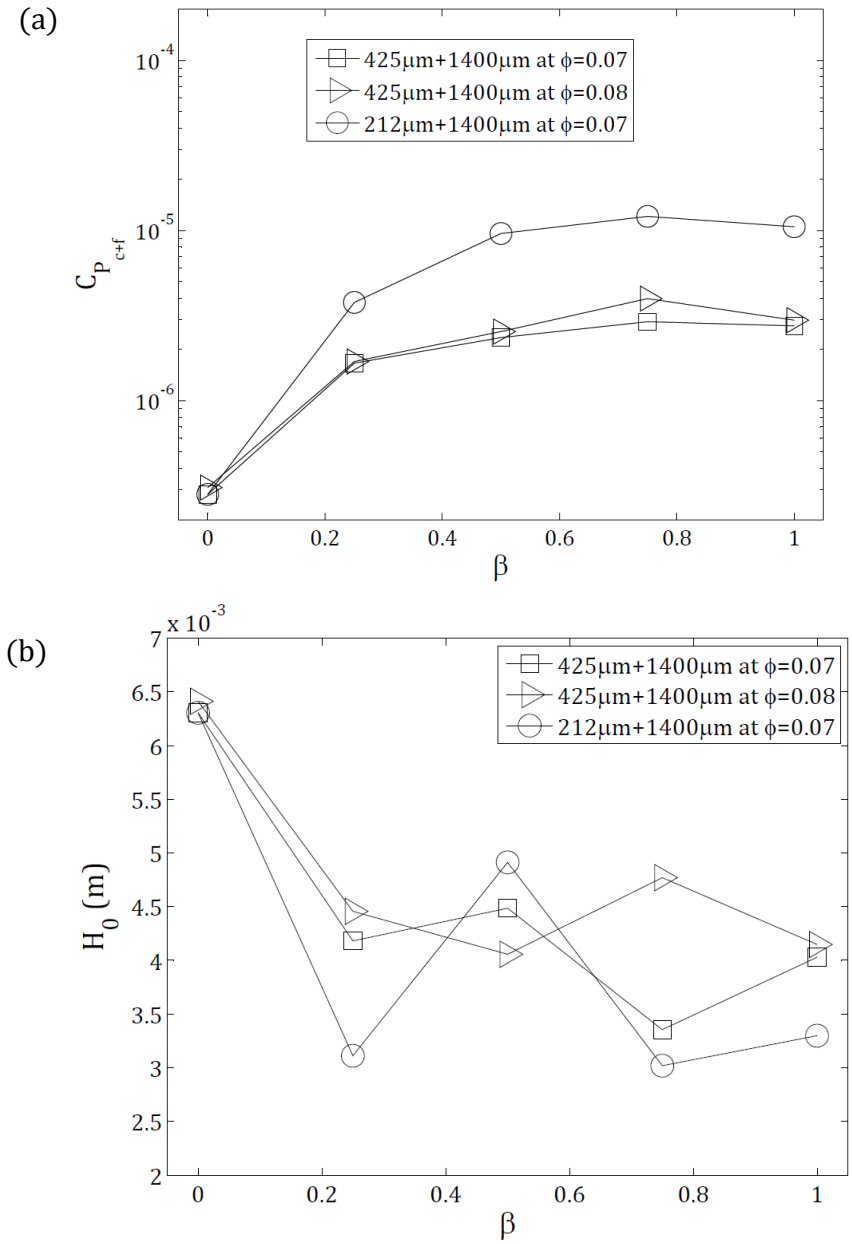

Figure 2.20: (a) Semi-log plot of *dynamic* permeability correction for cake layer $C_{P_{c+f}}$ v/s β for three different combinations of particles in bidisperse suspensions. (b) Plot of Height corresponding to capillary pressure loss H_0 v/s β for three different combinations of particles in bi-disperse suspensions.

2.5.3 *Discussion*

In this section some general data trends are discussed. Fig. 2.7 is a semi-log plot of packing density ρ_{pd} v/s ratio of settling tube width to particle size expressed as α. For the settling tube of width $b = 0.0153$ cm and particle sizes in our studies d_1, d_2 & d_3, the corresponding $\alpha = 10.93$, 36 & 72.17 respectively. By observing the trend shown in the plot, it can be observed that ρ_{pd} does not change significantly. This also means the value of void fraction(porosity) ϵ which is defined as $\epsilon = 1 - \rho_{pd}$, remains almost constant.

For mono-disperse suspensions of total solid concentration $\phi \leq 0.1$, Fig. 2.13 shows a typical comparison between experimental data for H_{bot} v/s t obtained from image analysis and numerical data for H_{bot} v/s t obtained from solving Eq. 2.2 by specifying the value of ω and H_{cmax}. This graph does not show the curves for just three different mono-disperse experiments and not all combinations. When we tried to extend this method to mono-disperse suspensions with total solid concentration $\phi > 0.1$, we observed that the numerical data was deviating from the experimental data. So for $\phi > 0.1$, we would need to develop a different equation for the cake height H_{bot}, which accommodates the deviations present in the current equation.

In Fig. 2.18, we can observe that for different initial guesses of the two variables marked as '$*$', the trajectories of optimization seem to follow unique paths. However, the final minimized value marked as '+' is the same for all the initial guesses. This can be observed in all four figures Fig. 2.18 (a) - (d), where (a) & (b) are error contours for filtration of mono-disperse suspensions and (c) & (d) are error contours for filtration of bi-disperse suspensions. This means, the pattern search algorithm seems to be robust in finding the global minimum for both the search variables.

For mono-disperse suspensions the *dynamic* permeability correction for the cake layer $C_{P_{c+f}}$ is supposed to increase with concentration because, thickness of cake layer is directly proportional to the total solid concentration ϕ. This means the resistance to fluid flow increases with concentration. Now, in the Fig. 2.19 (a) we can observe that numerically calculated $C_{P_{c+f}}$ increases with ϕ for three different particle species denoted by α_1, α_2 and α_3. From Fig. 2.19 (a) we can also observe that value of $C_{P_{c+f}}$ for α_3 is almost 10 times that of α_2 and value of $C_{P_{c+f}}$ for α_2 is almost 10 times that of α_1. So, it is clear that value of $C_{P_{c+f}}$ is dependent on the particle size d_P. We can say smaller the particle, higher is the *dynamic* permeability correction for the cake.

For bi-disperse suspensions, the *dynamic* permeability correction for the cake layer is dependent on total solid concentration ϕ and fraction of amount of small particle species in a bi-disperse mixture β. In Fig. 2.20 (a) the curves marked by '$\square$' and '$\triangleright$' correspond to ϕ = 0.07 & 0.08 respectively for bi-disperse mixture of particle species $d_1 = 1400$ μm and $d_2 =$ 425 μm where we can see that the value of $C_{P_{c+f}}$ increases with ϕ and β. So, for suspensions with $\beta > 0.5$, the value of $C_{P_{c+f}}$ tends to be more closer towards the one corresponding to a mono-disperse suspension smaller particles under study. The effect of particle size on the value of $C_{P_{c+f}}$ for bi-disperse suspensions is in agreement with the mono-disperse suspension.

In Fig. 2.19 (b) and 2.20 (b) we can observe that the change in height corresponding to capillary pressure loss is not greatly affected by ϕ or β seems to dominate for higher We also observe that $C_{P_{c+f}}$ value is affected by the fraction of small particles in a bi-disperse mixture β.

2.6 Conclusion

By experimentation, theoretical and numerical analysis, we found that the fluid flow experienced a constant pressure loss due to the permeability of the filter media, however the fluid flow experienced a increasing pressure loss due to cake permeability as a function of time. Experimental results for rate of cake formation showed a dependence on particle size d but not on the total solid concentration ϕ. Observation about the value of height corresponding to capillary pressure loss H_0 was seen not vary much with respect to either total solid concentration ϕ or particle size d. From this study we have determined that the *dynamic* permeability correction for cake layer $C_{P_{c+f}}$ is dependent on the total solid concentration ϕ and the size of the particle under study d_p. The time taken for complete filtration is higher for smaller particles and this can be attributed to reduction in porosity of the cake layer. Equation which explains cake layer height was limited to suspension concentrations $\phi < 0.1$, but this is due to limited flexibility of the equation and higher order terms if used, would easily explain the cake formation phenomena for higher concentrations. The fact these results are in close agreement with the findings of Lu *et al.* [44] is very promising.

CHAPTER 3. FUTURE WORK

3.1 Rheology of non-spherical particle suspensions

The rheological study of suspensions in this thesis has been limited to two different particle species. To answer the question of densely concentrated suspension behavior, one would need to analyze and identify all the parameters that affect the rheology of the system by experimenting on different size ratio and diverse particle size distribution. However, a more conclusive system would be to study the multi-disperse systems to account for understanding the effect of packing density.

3.2 Filtration of multi-disperse suspensions

To understand the behavior of filtration of a realistic suspension, one would need to analyze suspensions that are multi-disperse in nature with particle species of various relative & total concentrations, size and shape. By doing so, one can address suspensions of high concentrations $\phi > 0.1$, geometrical shapes other than spherical particles, and sizes beyond the range ($45\ \mu\text{m} \leq d \leq 1400\ \mu\text{m}$) studied in this work. Governing equations will needs to be updated when higher concentrations are used because the equation considered in this study for cake height is applicable for concentrations $\phi \leq 0.1$. Using the filtration data of mono-disperse suspensions, one can generalize the bi-disperse suspension parameters, but it is very important to calculate the permeability and packing density of the cake thus formed. So, a range of variables will need to be looked at in order to develop the physics that can describe the filtration of a realistic suspensions.

BIBLIOGRAPHY

[1] Albert Einstein. A new determination of molecular dimensions. *Ann. Phys*, 19(2): 289–306, 1906.

[2] Albert Einstein. *Investigations on the Theory of the Brownian Movement*. Courier Corporation, 1956.

[3] JS Chong, EB Christiansen, and AD Baer. Rheology of concentrated suspensions. *Journal of applied polymer science*, 15(8):2007–2021, 1971.

[4] H Eilers. The viscosity of the emulsion of highly viscous substances as function of concentration. *Kolloid-Zeitschrift*, 97(3):313–321, 1941.

[5] Vladimir Vand. Viscosity of solutions and suspensions. i. theory. *The Journal of Physical Chemistry*, 52(2):277–299, 1948.

[6] TB Lewis and LE Nielsen. Viscosity of dispersed and aggregated suspensions of spheres. *Transactions of The Society of Rheology (1957-1977)*, 12(3):421–443, 1968.

[7] Andrew P Shapiro and Ronald F Probstein. Random packings of spheres and fluidity limits of monodisperse and bidisperse suspensions. *Physical review letters*, 68(9):1422, 1992.

[8] CG d de Kruif, EMF Van Iersel, A Vrij, and WB Russel. Hard sphere colloidal dispersions: Viscosity as a function of shear rate and volume fraction. *The Journal of chemical physics*, 83(9):4717–4725, 1985.

[9] Norio Ouchiyama and Tatsuo Tanaka. Porosity of a mass of solid particles having a range of sizes. *Industrial & Engineering Chemistry Fundamentals*, 20(1):66–71, 1981.

[10] RK Gupta and SG Seshadri. Maximum loading levels in filled liquid systems. *Journal of Rheology (1978-present)*, 30(3):503–508, 1986.

[11] AJ Poslinski, ME Ryan, RK Gupta, SG Seshadri, and FJ Frechette. Rheological behavior of filled polymeric systems ii. the effect of a bimodal size distribution of particulates. *Journal of Rheology (1978-present)*, 32(8):751–771, 1988.

[12] V Fidleris and RL Whitmore. The physical interaction of spherical particles in suspensions. *Rheologica Acta*, 1(4-6):573–580, 1961.

[13] LCE Struik, HW Bree, and FR Schwarzl. Mechanical properties of highly filled elastomers v. Technical report, DTIC Document, 1966.

[14] CR Wildemuth and MC Williams. Viscosity of suspensions modeled with a shear-dependent maximum packing fraction. *Rheologica acta*, 23(6):627–635, 1984.

[15] RJ Farris. Prediction of the viscosity of multimodal suspensions from unimodal viscosity data. *Transactions of the Society of Rheology (1957-1977)*, 12(2):281–301, 1968.

[16] Melvin Mooney. The viscosity of a concentrated suspension of spherical particles. *Journal of colloid science*, 6(2):162–170, 1951.

[17] Fuzhong Qi and Roger I Tanner. Relative viscosity of bimodal suspensions. *Korea-Australia Rheology Journal*, 23(2):105–111, 2011.

[18] Jon Spangenberg, George W Scherer, Adam B Hopkins, and Salvatore Torquato. Viscosity of bimodal suspensions with hard spherical particles. *Journal of Applied Physics*, 116(18):184902, 2014.

[19] Philippe Gondret and Luc Petit. Dynamic viscosity of macroscopic suspensions of bimodal sized solid spheres. *Journal of Rheology (1978-present)*, 41(6):1261–1274, 1997.

[20] Jonathan J Stickel and Robert L Powell. Fluid mechanics and rheology of dense suspensions. *Annu. Rev. Fluid Mech.*, 37:129–149, 2005.

[21] Da He and Ndy N Ekere. Viscosity of concentrated noncolloidal bidisperse suspensions. *Rheologica acta*, 40(6):591–598, 2001.

[22] Fernando Concha and Raimund Bürger. Thickening in the 20th century: a historical perspective. *Minerals & metallurgical processing*, 20(2):57–67, 2003.

[23] JF Richardson. u. wn zaki: Sedimentation and fluidization. *Trans. Instn. chem. Engrs. Bd*, 32:35, 1954.

[24] BJ Konijn, OBJ Sanderink, and NP Kruyt. Experimental study of the viscosity of suspensions: Effect of solid fraction, particle size and suspending liquid. *Powder technology*, 266:61–69, 2014.

[25] HE White and SF Walton. Particle packing and particle shape. *Journal of the American Ceramic Society*, 20(1-12):155–166, 1937.

[26] RK McGeary. Mechanical packing of spherical particles. *Journal of the American ceramic Society*, 44(10):513–522, 1961.

[27] Henry Darcy. *Les fontaines publiques de la ville de Dijon: exposition et application...* Victor Dalmont, 1856.

[28] GO Brown. Henry darcy and the making of a law. *Water Resources Research*, 38(7), 2002.

[29] R Allan Freeze. Henry darcy and the fountains of dijon. *Ground Water*, 32(1):23–30, 1994.

[30] Edward W Washburn. The dynamics of capillary flow. *Physical review*, 17(3):273, 1921.

[31] George J Kynch. A theory of sedimentation. *Transactions of the Faraday society*, 48: 166–176, 1952.

[32] Frank M Tiller. Revision of kynch sedimentation theory. *AIChE Journal*, 27(5):823–829, 1981.

[33] Panayiotis Diplas and Athanasios N Papanicolaou. Batch analysis of slurries in zone settling regime. *Journal of environmental engineering*, 123(7):659–667, 1997.

[34] Mohammad Reza Garmsiri and Hassan Haji Amin Shirazi. A new approach to define batch settling curves for analyzing the sedimentation characteristics. *Journal of Mining and Environment*, 3(2):103–111, 2012.

[35] KE Davis, WB Russel, and WJ Glantschnig. Settling suspensions of colloidal silica: observations and x-ray measurements. *Journal of the Chemical Society, Faraday Transactions*, 87(3):411–424, 1991.

[36] Frank M Tiller, NB Hsyung, and DZ Cong. Role of porosity in filtration: Xii. filtration with sedimentation. *AIChE Journal*, 41(5):1153–1164, 1995.

[37] Richard Wakeman. The influence of particle properties on filtration. *Separation and Purification Technology*, 58(2):234–241, 2007.

[38] Peter B Sørensen, Per Moldrup, and Jensaa Hansen. Filtration and expression of compressible cakes. *Chemical Engineering Science*, 51(6):967–979, 1996.

[39] Raimund Bürger, Fernando Concha, and K Hvistendahl Karlsen. Phenomenological model of filtration processes: 1. cake formation and expression. *Chemical Engineering Science*, 56(15):4537–4553, 2001.

[40] R Font and A Hernández. Filtration with sedimentation: Application of kynchs theorems. *Separation Science and Technology*, 35(2):183–210, 2000.

[41] Chi Tien, Renbi Bai, and BV Ramarao. Analysis of cake growth in cake filtration: Effect of fine particle retention. *AIChE journal*, 43(1):33–44, 1997.

[42] Azad Kavoosi. *Investigating the Fundamental Parameters of Cake Filtration using a Gravity Column Device*. PhD thesis, 2014.

[43] SCA França, G Massarani, and EC Biscaia. Study on batch sedimentation simulation—establishment of constitutive equations. *Powder technology*, 101(2):157–164, 1999.

[44] Wei-Ming Lu, Kuo-Lun Tung, Chun-Hsi Pan, and Kuo-Jen Hwang. The effect of particle sedimentation on gravity filtration. 1998.

[45] Morten Lykkegaard Christensen and Kristian Keiding. Numerical model of gravity drainage of compressible organic slurries. *Powder technology*, 217:189–198, 2012.

[46] Monika Bargieł and Elmer M Tory. An extension of the particle-based approach to simulating the sedimentation of polydisperse suspensions. *International Journal of Mineral Processing*, 79(4):235–252, 2006.

[47] Louis Hernando, Aziz Omari, and David Reungoat. Experimental investigation of batch sedimentation of concentrated bidisperse suspensions. *Powder Technology*, 275:273–279, 2015.

[48] Alexia Grenier, Martine Meireles, Pierre Aimar, and Philippe Carvin. Analysing flux decline in dead-end filtration. *Chemical Engineering Research and Design*, 86(11):1281–1293, 2008.

[49] Albert Rushton, Anthony S Ward, and Richard G Holdich. *Solid-liquid filtration and separation technology*. John Wiley & Sons, 2008.

[50] Ladislav Svarovsky. *Solid-liquid separation*. Butterworth-heinemann, 2000.

[51] Siegfried Ripperger, Walter Gösele, Christian Alt, and Thomas Loewe. Filtration, 1. fundamentals. *Ullmann's Encyclopedia of Industrial Chemistry*.

[52] Sung-sam Yim. A theoretical and experimental study on cake filtration with sedimentation. *Korean Journal of Chemical Engineering*, 16(3):308–315, 1999.

[53] Raimund Bürger and Wolfgang L Wendland. Sedimentation and suspension flows: Historical perspective and some recent developments. *Journal of Engineering Mathematics*, 41(2-3):101–116, 2001.

[54] Patrick Snabre, Bernard Pouligny, Cyrille Metayer, and François Nadal. Size segregation and particle velocity fluctuations in settling concentrated suspensions. *Rheologica acta*, 48(8):855–870, 2009.

[55] Peter A Smith and Richard A Haber. Effect of particle packing on the filtration and rheology behavior of extended size distribution alumina suspensions. *Journal of the American Ceramic Society*, 78(7):1737–1744, 1995.

[56] RI Mackie and Q Zhao. A framework for modelling removal in the filtration of polydisperse suspensions. *Water Research*, 33(3):794–806, 1999.

[57] Frank M White and Isla Corfield. *Viscous fluid flow*, volume 3. McGraw-Hill New York, 2006.

[58] Gary E Mueller. Radial void fraction distributions in randomly packed fixed beds of uniformly sized spheres in cylindrical containers. *Powder technology*, 72(3):269–275, 1992.

[59] Andrew R White and Thomas Ward. Pattern search methods for pendant drops: Algorithms for rapid determination of surface tension and surfactant transport parameters. *Colloids and Surfaces A: Physicochemical and Engineering Aspects*, 485:1–10, 2015.